New interpretations of upstream migration of bedform(Dissertation_全文)

AUTHOR(S):

Kubo, Yusuke

New interpretations of upstream migration of bedforms

1999

by Yusuke Kubo

Abstract

It is known that some bedforms developing on a bed under unidirectional flow can migrate upstream against the flow, while most bedforms migrate downstream with the flow. The migration of bedforms has been considered to result from steady but differential deposition due to different flow conditions on both sides of the bed undulation. This thesis provides new interpretations of upstream migration of bedforms including shallow water antidunes and deep water sediment waves.

Antidunes are formed in quick flow such as rivers and beaches, with typical wavelengths of decimeters to meters. A cycle of events is observed in antidune sedimentation, which begins with a smooth flow and ends with a breaking of water surface waves. The wave breaking, as well as the differential deposition, gives rise to upstream migration of antidunes and to lens-like sedimentary structures in sand-sized sediments. This cycle of events can be interpreted as successive formation and collapse of a hydraulic jump, caused by growth and destruction of antidunes. The theoretical considerations in this thesis quantify the process of erosion, transport and deposition of sediments by the hydraulic jump on the upstream side of the antidune, based on hydraulics of the flow over an obstacle. It is shown that the variation of the flow pattern is consistent with the laboratory observations of the cycle of events.

The mechanism of formation of deep sea sediment waves, with typical wavelength of kilometers, by turbidity currents is yet to be understood. This thesis attempts to prove an assumption that the large scale wavy topography is produced by preferential deposition from turbidity currents after a change of slope, both from laboratory experiments and numerical simulations. Topographic effects on deposition from turbidity current are investigated in laboratory experiments, and the results show that the preferential deposition actually takes place after a slope break in a flume. It is also shown that the differential deposition occurs on both sides of the wavy topography, implying the inevitable upstream migration of sediment waves produced by turbidity currents.

The numerical simulation based on layer-averaged Navier-Stokes equations successfully predicts the experimental results, and applied to turbidity currents in nature. The comparison of the model predictions with the experimental results shows that the preferential deposition is not caused by specific fluid motions such as hydraulic jump and lee-waves but by topographic effects on deposition from turbidity currents. The numerical model is then applied to sediment wave formation by spillover turbidity currents on abyssal levees. The model predicts the development of wavy structures after accumulation of thousands of turbidite beds on an initially flat bed. The wave formation is initiated by preferential deposition after a change of slope and developed as a train of individual mounds. The wavy structures in the model predictions have similar features to those of natural sediment waves for the length scale, waveform and the pattern of internal layering, and are interpreted to show the process of sediment wave formation by turbidity currents near a submarine channel.

Contents

§I. Introduction

It is widely known that wave-like bedforms are developed in unidirectional flow. The bedforms move either upstream or downstream with lower velocities than the flow velocity, and the migration leads to the development of various stratification features in sedimentary structures. The direction of bedform migration is, therefore, the most essential factor in analyzing paleocurrent direction from the sedimentary structures. It is of great importance to understand the mechanism of bedform migration in order to extract various kinds of information and to interpret ancient depositional environments from geological records.

Upstream migration of bedforms has been known to occur in shallow water, though it is less common than downstream migration of ripples and dunes. Gilbert (1914) observed this unusual bedform in open channel flume experiments and named it "antidune" after its possible upstream migration. Antidunes are formed under high flow intensities of the upper flow regime and are commonly observed in natural rivers and beaches, though rarely found as relict bedforms in ancient rocks. Antidunes are characterized by their symmetrical waveform with a typical wavelength of a decimeter to meters, and by the water surface waves which either tend to break frequently, or are almost stationary and in-phase with the bed waves.

The upstream migration of antidunes takes place as a result of differential deposition on the upstream and downstream flanks of the bed undulation. Kennedy (1963) successfully quantified this process based on the assumption that the antidune configuration should correspond to a streamline of the flow at the bed, and obtained a stability field for the upstream migrating antidunes. While the steady but differential deposition has been focused on in theoretical considerations on antidunes, it has been observed in some experimental studies that the breaking of water surface waves can give rise to the upstream migration of antidunes (e.g., Gilbert, 1914; Middleton, 1965). The breaking of waves, however, has been almost ignored in theoretical considerations of antidune sedimentation, despite its common occurrence and importance as the process responsible for

bedform migration.

Another example of upstream migration of bedforms has been reported from deep-sea sediment waves. Deep-sea sediment waves, with typical amplitudes of tens of meters and wavelengths of several kilometers, have a subsurface layering indicating upstream migration of the waves, which has invoked analogies with fluvial antidunes (e.g. Fox *et al.*, 1968). Sediment waves have been reported from various environments, from continental slopes to abyssal plains, and several processes have been proposed as the mechanism of sediment wave formation, including antidunes, slumping or sliding, gullying and lee waves formed in bottom currents (Allen, 1982b).

The upstream migration of sediment waves has been successfully modeled by Flood (1988), based on differential deposition caused by lee waves in steady bottom currents. However, there are many reports of sediment wave fields on the back slopes of levees of submarine channels (e.g. Normark *et al.*, 1980; Nakajima, 1996). These sediment waves are interpreted as depositional bedforms produced by turbidity currents which spilled out from the submarine channel. Although these waves display similar features as those produced by continuous bottom currents, the currents responsible for their formation are of a different nature: turbidity currents are shorter-lived and have larger Froude numbers than continuous bottom currents. It is unlikely that sediment waves are developed in the same way by these different flows. The mechanism of sediment wave formation by turbidity currents is yet to be understood.

The purpose of this thesis is to model the unknown processes of upstream migration of bedforms. A review of previously established models of the bedform migration is given and the processes of breaking of waves on antidunes and of sediment wave formation on submarine levees are looked at. A theoretical description of the breaking of waves is presented in chapter 2 and sediment wave formation is described in chapter 3 using results from experimental and numerical studies of turbidity currents.

§.2 Breaking of waves on antidunes

2.1 Antidunes

Antidunes are bedforms produced under high flow intensities of the upper flow regime, and are characterized by upstream migration against the flow. The possible upstream migration of antidunes is in contrast with downstream migration of other wavy bedforms such as dunes and ripples, and is due to formation of upstream-dipping laminae on the stoss side of the bed undulations. Gilbert (1914) originally defined antidunes as upstream-migrating sinusoidal bed waves, which tended to be broadly in-phase with the water surface. While the phase equivalence has been preferred in the definition of antidunes since Kennedy (1963), upstream migration is unique to antidune bedforms.

Antidunes are accompanied by water surface waves, which tend to break rather frequently and are broadly in-phase with the bedforms. The in-phase waves have been analyzed as deep-water waves, assuming that the moving bed waves correspond to the streamline of the flow at the bed (e.g. Kennedy, 1963; Allen, 1982a). The theoretical study of Kennedy (1963) showed that bedform migration was due to differential deposition on the stoss and the lee side of the bed waves, and obtained a stability field for upstream migrating bed waves. The relaxed expressions of the stability field, which are similar to the equation for the deep-wave celerity, have been used by geologists attempting estimations of paleocurrent conditions from antidune bedforms preserved in geological records (e.g., Walker, 1967; Hand *et al.*, 1969; Skipper, 1971). Reynolds (1965) and Kennedy (1969) corrected weaknesses in Kennedy's (1963) analysis. Hand (1969) employed trochoidal waves to describe antidune profiles, and estimated the maximum flow depth from ancient antidune profiles.

Antidunes are rarely found as relict bedforms in ancient rocks, while active antidunes have been commonly observed in steep or shallow streams in nature (Allen, 1982a). It is generally thought that antidune bedforms are rapidly destroyed and their cross stratification are unlikely to be

preserved. However, there have been reports of antidune structures in geological records (Walker, 1967; Hand *et al.*, 1969; Skipper, 1971; Skipper and Bhattacharjee, 1978; Schmincke *et al.*, 1973; Fralick, 1999). Antidunes have also been inferred as an origin of decimeter-scale hummocky cross - stratification (HCS) in ancient beds (Prave and Duke, 1990; Yagishita, 1994; Rust and Gibling, 1990).

These interpretations of ancient antidunes, however, have been questioned in some cases. Allen (1982a) suggested that Walker's (1967) undulations were subparallel with paleocurrents and were related to secondary flow during aggradation. Pickering and Hiscott (1985) reinterpreted the cross-stratification in the Cloridorme Formation (Canada) as deposits from contained (reflected) turbidity currents. Unfortunately, a criterion to identify antidune sedimentation in geological records is yet to be established.

Antidunes have been intensively studied in laboratory flumes since Gilbert (1914), and a stability field for antidunes has been established empirically. The experimental data, as well as field observations, showed good agreement with Kennedy's (1963) model for antidune wavelength as a function of flow conditions (see Allen, 1982a for review). The processes involved in antidune sedimentation and the resultant internal structures were described in the experimental study of Middleton (1965). Hand (1974) succeeded in producing antidune structures in a two-layer flow system.

Most of the experimental studies, together with field observations of active antidunes, have inferred the breaking of water surface waves (e.g. Middleton, 1965). The stationary waves on the free water surface develop in-phase with antidunes and tend to break rather frequently. The breaking waves interact so strongly with the bed as to "obliterate the antidunes and level the bed" (Kennedy, 1963). Several authors have pointed out that the breaking of waves, as well as the differential deposition, can give rise to upstream migration of antidunes (Middleton, 1965; Allen, 1966; 1982a). The mechanism of the breaking of waves, however, has been focused on less in antidune sedimentation, despite its importance as a reworking process of bed configuration and as a

secondary process involved in the upstream migration of antidunes.

In this chapter, a theoretical description of the process of wave-breaking on antidunes is presented based on observations of antidunes formed on sand beds in open-channel laboratory flumes. Hydraulics of the flow over an obstacle are explored to quantify the flow conditions for breaking antidunes. General consideration is given to deposition caused by the breaking of waves, and the applicability of the model to antidunes formed in turbidity currents is then discussed.

2.2 Descriptions of the breaking of waves

There have been many descriptions of antidunes since Gilbert (1914), mainly based on experiments on sand beds in open-channel laboratory flumes. It has been commonly observed that the breaking of water surface waves occurs rather frequently and cyclically, and is associated with destruction and reestablishment of antidunes (Middleton, 1965; Allen, 1966; 1982a; Yokokawa *et al.*, 1999). Middleton (1965) described the process of wave breaking on antidunes in a laboratory flume. He indicated that the wave breaking, as well as the differential deposition, gave rise to upstream migration of antidunes and to lens-like sedimentary structures in sand-sized sediments. Allen (1966) identified four modes of deposition from antidunes, one of which is characterized by the breaking water waves and resultant upstream-dipping laminae. According to these authors, a series of events is observed in antidune sedimentation, which begins with a smooth flow and ends with breaking of water surface waves.

Fig. 2.1. Converted pictures of the breaking of waves on an antidune, captured at 0.1 sec intervals. Flow is from right to left. Darker color indicates higher concentration of sediment. Note the upstream transportation of sediment by the breaking wave and establishment of a new antidune upstream of the old one. Reproduced from Yokokawa *et al.* (1999). See the original article for details.

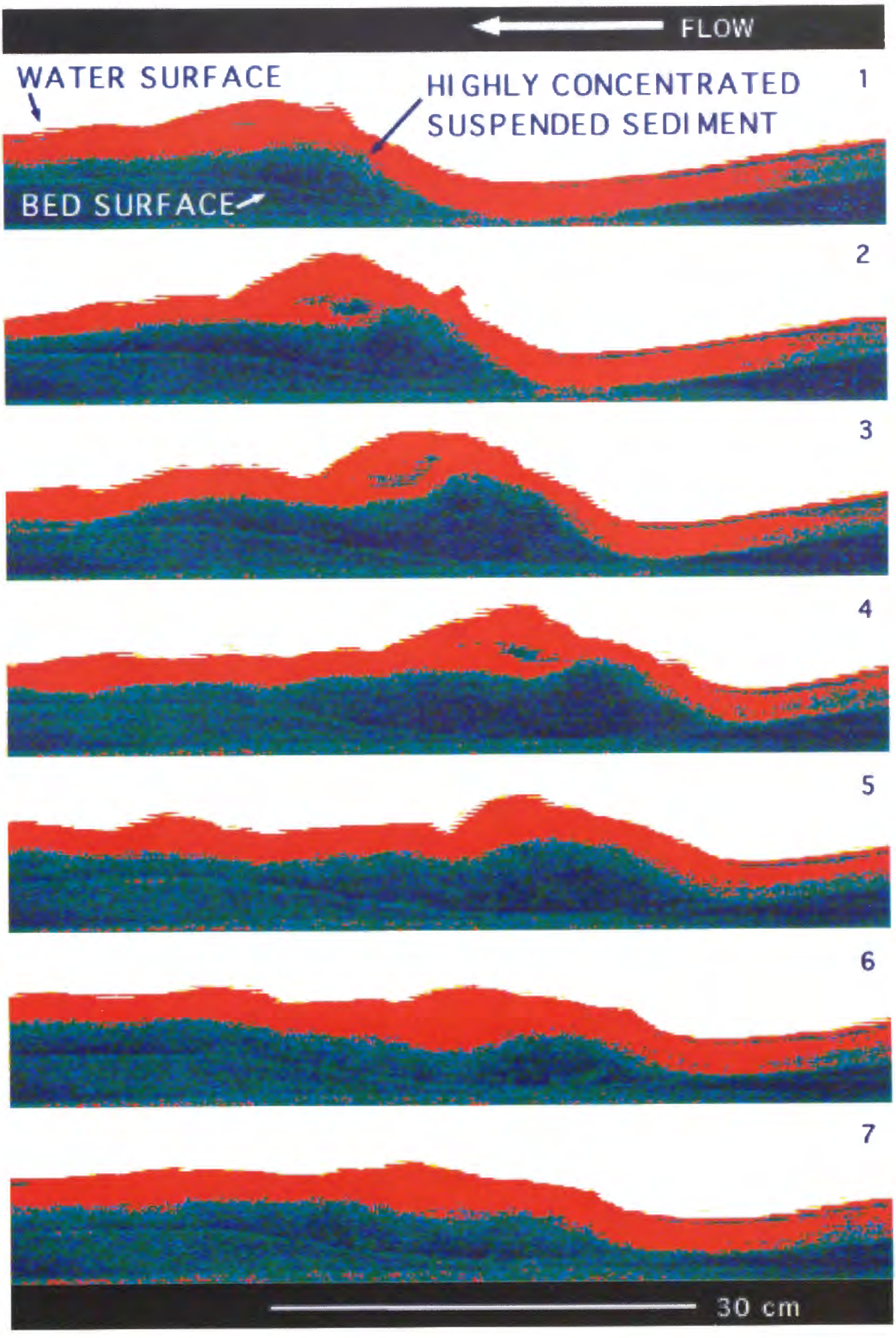
FLOW
WATER SURFACE
HIGHLY CONCENTRATED
SUSPENDED SEDIMENT
BED SURFACE
1
2
3
4
5
6
7
30 cm

Figure 2.1 shows the typical sequence of events observed in laboratory experiments of antidunes (Yokokawa *et al.*, 1999). Antidunes and water waves, which are initially in-phase and almost stationary, grow in size under a smooth flow. The growing antidunes then disturb the smooth passage of the flow. The flow becomes unstable, and breaking of the water wave takes place on the upstream flank of the associated antidune. Just before breaking, the wave moves upstream generating intense turbulence. A great cloud of sediment is taken into suspension, and a substantial part surges upstream with the breaking wave and contributes to the establishment of a new antidune somewhat upstream of the old one. The flow is smooth again with the formation of the new antidune and returns to the start of the cycle.

2.3 Modeling

In order to describe this sequence of events repeated in antidune sedimentation, hydraulics of the flow in the vicinity of a mound are looked at (Fig. 2.2). It is assumed that the mound is fixed in space laterally but the height is variable due to erosion and deposition.

Smooth flow

Antidunes grow in size under a smooth flow (Fig. 2.2a). The flow velocity u_c and depth d_c at the crest of the mound are determined from those on the upstream side, u_a and d_a, by

$$\frac{u_a^2}{2} + gd_a = \frac{u_c^2}{2} + g(d_c + z) \tag{2.1}$$

$$u_a d_a = u_c d_c \tag{2.2}$$

where z is the height of the mound, g is the acceleration due to gravity, and subscriptions represent locations. Equation (2.1) describes conservation of energy and is derived from the Bernoulli equation, and eq. (2.2) represents mass conservation. Using the Froude number $Fr = u/(gd)^{1/2}$ instead of the flow velocity, eqs. (2.1) and (2.2) are unified as

(a) smooth flow

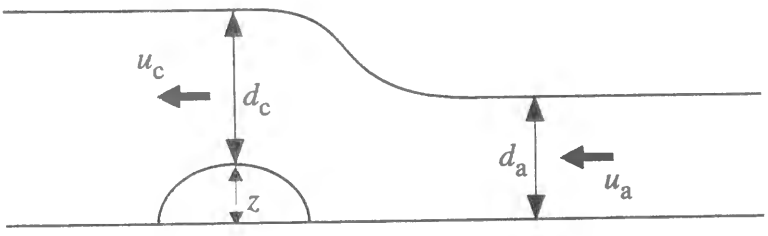

(b) hydraulic jump

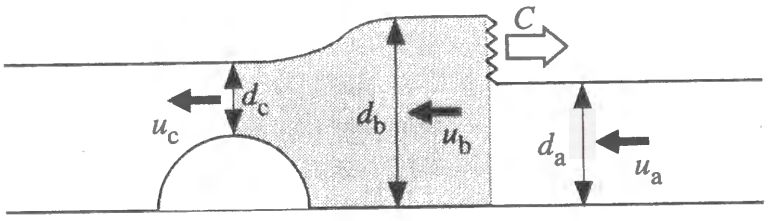

(c) deposition

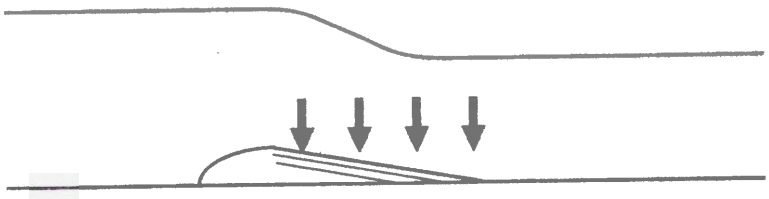

Fig. 2.2. Definition sketches for notation for typical sequence of events in antidune sedimentation. (a) Smooth flow with a mound; (b) Hydraulic jump moving upstream; (c) Deposition on the upstream side of the mound.

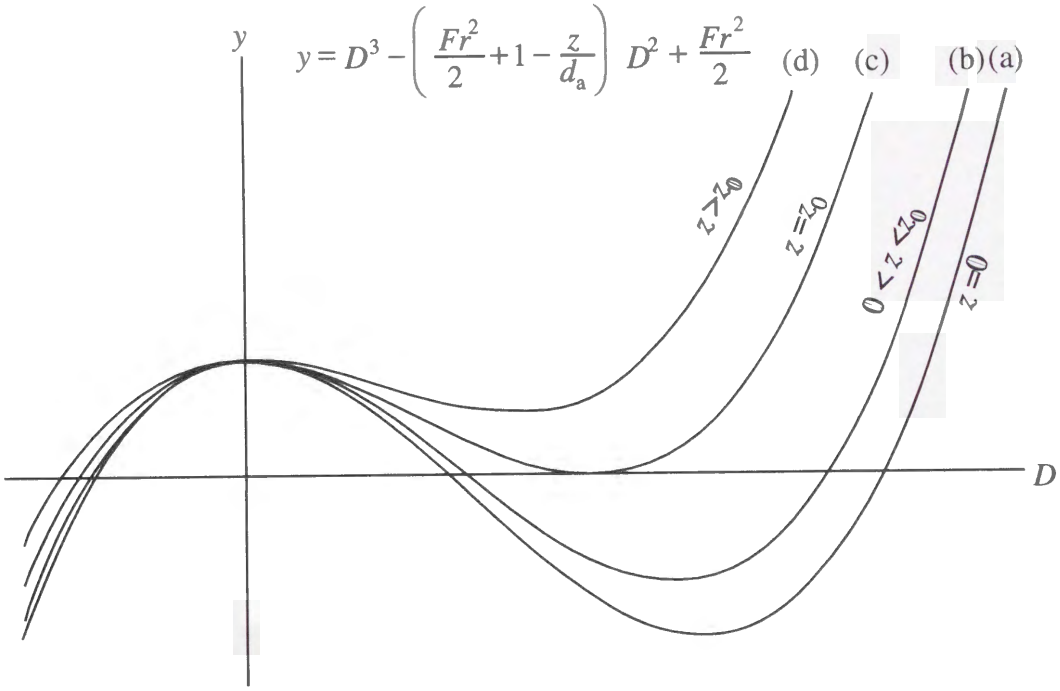

Fig. 2.3. The cubic expression for the left-hand side of eq. (2.3), shown for four different values of the height of the topographic elevation, z. (a) Eq. (2.3) has positive solutions for z =0; (b) The solutions are changed as a slight z is induced; (d) Eq. (2.3) has no real solutions for positive D for sufficiently large z through the critical condition (c) determined by eq. (2.4).

$$D^3 - \left(\frac{Fr^2}{2} + 1 - \frac{z}{d_a} \right) D^2 + \frac{Fr^2}{2} = 0 \qquad (2.3)$$

where $D = d_c/d_a$ is the dimensionless flow depth. The Froude number represents the ratio of the flow velocity divided by the maximum wave celerity. Flow is termed supercritical or subcritical when its Froude number is larger or smaller than unity, respectively.

Equation (2.3) gives the change of the flow depth on the mound. When the bed is flat ($z = 0$), eq. (2.3) has solutions for positive D as (Fig. 2.3a),

$$D = 1$$

$$D = \left(1 + \sqrt{1 + \frac{8}{Fr^2}} \right)$$

The first solution ($D = 1$) obviously yields no changes in the flow conditions. The value of the second solution becomes larger than unity ($d_c > d_a$) in a supercritical flow ($Fr_a > 1$) and smaller than unity ($d_c < d_a$) in a subcritical flow ($Fr_a < 1$). A transition of the flow depth between the two solutions is called a hydraulic jump in a supercritical flow or hydraulic drop in a subcritical flow.

With the mound on the bed, the solutions for D are changed with the height of the mound, z (Fig. 2.3b). In a supercritical flow, the two solutions for D both become larger than unity ($d_c > d_a$). The water surface is, therefore, in-phase with the bed topography, and the flow velocity is decreased on the mound. The deceleration, and the resultant difference of the rate of erosion (or deposition), is likely to further increase the vertical height of the mound on an erodible bed.

In a subcritical flow, the two solutions for D both become smaller than unity ($d_c < d_a$). The flow becomes faster and thinner on the mound. The mound is unlikely to grow in size due to the larger rate of erosion on the mound.

When the mound grows sufficiently large in a supercritical flow, eq. (2.3) has no real solutions for positive D (Fig. 2.3d). The critical condition (Fig. 2.3c) is expressed as

$$z_0 = d_a\left(\frac{1}{2}Fr_a^2 - \frac{3}{2}Fr_a^{2/3} + 1\right)$$
$$Fr_c = 1 \qquad (2.4)$$

where z_0 is the critical height of the mound.

hydraulic jump

When the height of the mound exceeds the critical value, z_0, eq. (2.3) yields no appropriate solutions. The flow can no longer attain the smooth and steady conditions so that a hydraulic jump with energy loss must form on the upstream side of the mound (Fig. 2.2b) (Long, 1954). While the flow dynamics are complicated due to the turbulent and unstable nature of the hydraulic jump, a simple description for such flow is obtained by assuming the flow to be hydrostatic except at the jump with conservation of momentum (e.g. Baines, 1995), as

$$(u_a + c)d_a = (u_b + c)d_b \qquad (2.5)$$

$$u_b d_b = u_c d_c \qquad (2.6)$$

$$(u_a + c)^2 = \frac{gd_b}{2}\left(1 + \frac{d_b}{d_a}\right) \qquad (2.7)$$

$$\frac{u_b^2}{2} + gd_b = \frac{u_c^2}{2} + g(d_c + z) \qquad (2.8)$$

$$u_c^2 = gd_c \qquad (2.9)$$

where c is the adverse speed of the jump. Equations (2.5) and (2.6) represent mass conservation. Equation (2.7) represents momentum conservation through the hydraulic jump. Equation (2.8) is the Bernoulli equation behind the jump. Equation (2.9) is the critical condition at the crest of the mound. The solution of these equations is shown in Fig. 2.4 for the upstream jump speed rendered dimensionless by

$$C = \frac{c}{\sqrt{gd_a}}$$

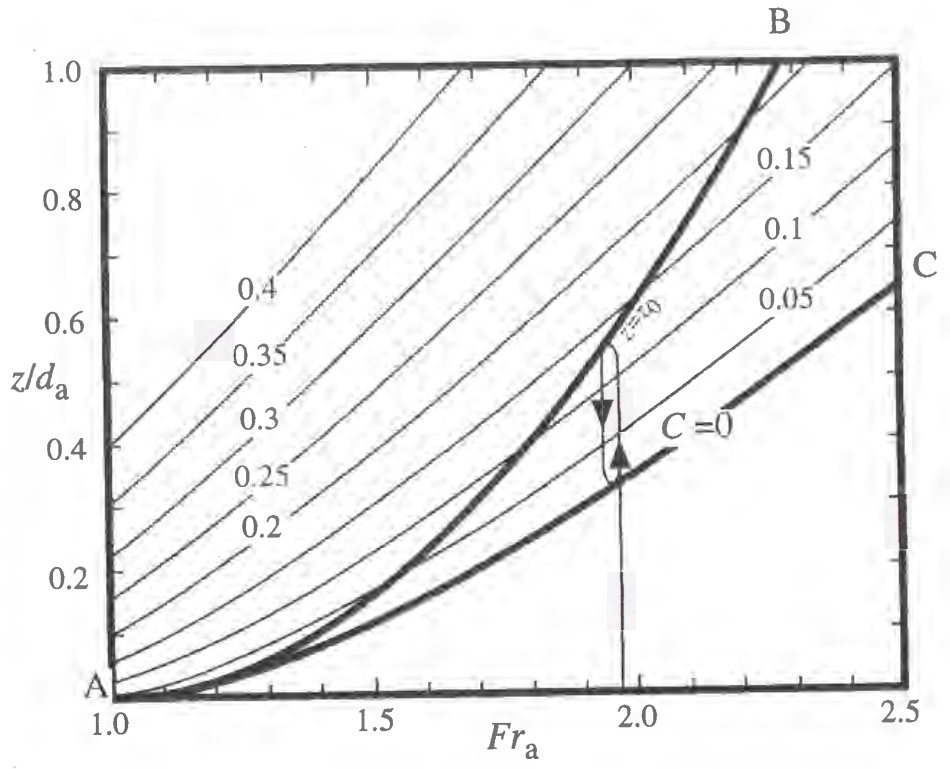

Fig. 2.4. Relative height of the mound (z/d_a) as a function of upstream Froude number (Fr_a) calculated from eq. (2.4) for different values of dimensionless jump speed, $C = c/(gd_a)^{1/2}$. Hysteresis is observed within region BAC determined by $z = z_0$ in eq. (2.4) and $C = 0$.

Within region BAC in Fig. 2.4, the flow can be either supercritical everywhere or accompanied by an upstream jump (Baines, 1995). The possibility of two states implies that there is hysteresis in the system, which seems to be consistent with a cycle of events observed in antidune sedimentation. Assuming that the height of the mound is increased in a supercritical flow and decreased in a subcritical flow, the flow conditions should be expected to show the following temporal changes.

When the height of the mound exceeds its critical value (curve AB), a hydraulic jump is formed at the crest of the mound. The jump moves upstream ($c>0$), and a subcritical flow is imposed between the jump and the mound. In the subcritical flow, however, the mound tends to be depressed because of differential erosion or deposition. The height of the mound is decreased until the jump becomes stationary relative to the mound (curve AC). Destruction of the mound is possibly promoted by turbulence generated within the stationary or slowly migrating hydraulic jump. The hydraulic jump disappears when the height of the mound is further depressed and the jump speed becomes negative. After the disappearance of the hydraulic jump, which has been mentioned as the breaking of waves, the flow is again supercritical everywhere and returns to the start of the cycle.

After the disappearance of the hydraulic jump, which has been mentioned as the breaking of waves, the destructed mound is left in the flow which is again supercritical everywhere. Even though the mound has been fully destructed, a slight irregularity of the bed can lead to form a new mound in a supercritical flow. Therefore, the flow conditions return to the start of the cycle with a new mound.

Deposition caused by the hydraulic jump

Through the above cycle of events, upstream transport of sediment can take place in the vicinity of the mound. Part of the sediment eroded from the mound is held in suspension by turbulence within the hydraulic jump, and is transported along with the upstream migrating jump. As the

hydraulic jump disappears (Fig. 2.2c), the suspended sediment is deposited on the upstream side of the mound, resulting in the possible formation of upstream-dipping laminae on the upstream flank or lenticular structures in the troughs.

It should be noted, however, that a weak hydraulic jump is unlikely to contribute to upstream transport of sediments. The hydraulic jump in a flow with Froude number near unity is almost steady ($C \cong 0$) and disappears by slight erosion at the crest of the mound. The flow is expected to be fairly stable, so differential deposition would be the dominant process in the development of antidunes. In fact, a hydraulic jump is formed as a smooth undular bore when the change of Froude number through the jump is slight (Binnie and Orkney, 1955; Baines, 1995). The observed structures of bores are described as smooth when the upstream Froude number $Fr_a > 1.26$, partially turbulent when $1.26 < Fr_a < 1.55$ and fully turbulent when $Fr_a > 1.55$ (Binnie and Orkney, 1955).

Sedimentary structures formed by the hydraulic jump can possibly be identified in antidune stratification, if enough sediment is transported and deposited. Deposition takes place both on the upstream flank and in troughs of antidunes, depending on the position where the hydraulic jump disappears. Deposits caused by the breaking of waves, therefore, might not show a direct relationship with the wavelength of antidunes. Middleton (1965) observed in his flume experiments that the breaking of waves gave rise to lens-like structures whose length was somewhat shorter than the wavelength of the antidunes. Hand *et al.* (1969) found partial filling of the troughs in antidune structures in the Mount Toby conglomerate, and attributed it to deposition by the breaking waves. He showed that groups of steep antidunes were separated by other less-steep antidunes, and suggested the less-steep antidunes marked places of wave breaking.

Application to density currents

It is possible that a hydraulic jump is formed at a fluid interface in two- or multi-layer systems (Baines, 1988). Experimental work of Hand (1974) showed that antidunes and associated breaking waves were formed by density currents in two-layer systems. While the upper and lower fluids

interact in a complicated way in the turbulent hydraulic jump, the simplest approach to describe the two-layer systems in which the overlying fluid is sufficiently deep and at rest is to replace the Fr_a in Fig. 2.4 by the densiometric Froude number $Fr_d = u/(g' d)^{1/2}$, where $g' = (\Delta\rho/\rho)g$ represents reduced gravity, ρ is the density of the underflow and $\Delta\rho$ is the density difference between the underflow and overlying fluid (Komar, 1971). Figure 2.4 predicts that a similar process of wave breaking (hydraulic jump) should be observed at the upper interface of the underflow.

There are several reports of antidune structures in turbidite beds (e.g. Walker, 1967; Skipper, 1971; Prave and Duke, 1990; Yagishita, 1994). The inferences of antidunes are, however, commonly questioned based on hydrodynamic reasons (e.g. Pickering and Hiscott, 1985). From the theoretical considerations of Hand *et al.* (1972), it follows that antidunes in two-layer systems have wavelength (L) to flow depth (d) ratios of $L/d > 12.6$, implying a centimeter-scale flow thickness for decimeter-scale antidunes. In order to explain the small flow thickness, Hand *et al.* (1972) suggested that the antidunes in turbidites might be attributed to a thin internal layer of a differing density within the turbidity current. The solutions in Fig. 2.4 and the considerations on generation of turbulent hydraulic jump also suggest that the flow depth should be the same order as the antidune heights.

2.4 Discussion

The sequence of events observed with breaking of waves on antidunes is successfully described as formation and disappearance of a hydraulic jump in a supercritical flow. The solutions obtained are, however, are only approximate because of the assumptions involved in the derivation of the equations and the simplifications in the descriptions of the systems in the vicinity of the mound.

Only a single mound has been considered in this study, whereas antidunes are a train of such mounds on a relatively steep slope. The model must be extended to a curvilinear and sloped bed to

include quantitatively the features of antidune configurations, because the flow conditions are dependent on the shape of the mound and the profile of antidunes. It should be emphasized though, that the formation of a hydraulic jump is essentially determined by the height of the mound and independent of the wavelength or waveform of antidunes, if the incoming flow is steady.

The conditions of the incoming flow are continuously changed with the growth and the decay of the front mound. When the flow accelerates on the lee-side downslope of the front mound, the incoming flow will attain a higher Froude number locally and temporarily than the average value. Such variation of flow conditions is likely to result in further development of antidunes and a possible hydraulic jump. The flow conditions for the formation of the hydraulic jump should not be determined only by average flow conditions.

The dynamics of a hydraulic jump are well understood as an upstream effect generated by an obstacle in a stratified flow (for a review see Baines, 1995). However, the turbulent and unstable hydraulic jump on an erodible bed can not be described quantitatively. Further investigations are required to quantify the interaction of the hydraulic jump with the bed configuration and to obtain the relationship with sedimentary structures.

§3. Sediment wave formation by turbidity currents

3.1 Deep-sea sediment waves

Deep-sea sediment waves are regular bed undulations on a relatively large scale, with typical amplitudes of tens of meters and wavelengths of a few kilometers. The crest lines are continuous over tens of kilometers and are generally normal to or at a small angle to the current direction (cf. Blumsack and Weatherly, 1989). The subsurface layering generally indicates upstream wave migration, but occurrences of downstream migration have been observed (Roberts and Kidd, 1979). The possible upstream migration has invoked analogies with fluvial antidunes to some workers (Fox *et al.*, 1968; Normark *et al.*, 1980; Piper and Savoye, 1993). Deep-sea sediment waves have been reported from a wide range of settings, from continental slopes to abyssal plains, and, based on their regular shape and continuous internal layering, are generally interpreted as depositional and/or erosional features created by submarine flow activities. Both alongslope thermohaline currents and downslope turbidity currents are thought to be responsible for wave formation.

In most cases, sediment waves have been interpreted as bedforms created by thermohaline flow (e.g. contour currents) within the benthic boundary layer. The broad regional extent of the wave fields, which are often restricted to narrow depth ranges yet extend long distances parallel to regional contours, has generally been regarded as a primary indicator of contour current deposition. Such wave fields include the lower continental rise hills in the northeastern Atlantic (Brew and Mayer, 1998; Fox *et al.*, 1968; Markl *et al.*, 1970; Rona, 1969; Driscoll and Laine, 1996), the Rockall Trough in the northwestern Atlantic (Howe, 1996; Richards *et al.*, 1987; Roberts and Kidd, 1979; Stoker *et al.*, 1998), the Argentine Basin (Ewing *et al.*, 1971; Klaus and Ledbetter, 1988; Flood and Shor, 1988; Flood *et al.*, 1993), the Brazilian Basin and the East Brazilian Margin (Damuth, 1975; Damuth and Hayes, 1977), the Vema Channel (Johnson, 1984; Johnson *et al.*,

1984), the Bonin Trough in the western Pacific (Jacobi and Mrozowski, 1979), the Indian ocean (Johnson and Damuth, 1979; Kolla *et al.*, 1976), the margin of Africa (Egloff, 1972; Jacobi *et al.*, 1975; Kolla *et al.*, 1980), the margin of Antarctica (Tucholke, 1977; Kuvaas and Leitchenkov, 1992; Gilbert *et al.*, 1998; Howe *et al.*, 1998), the Arctic Ocean (Hall, 1979), the Central Basin of the Pacific (Lonsdale and Smith, 1980) and in the Mediterranean (Marani *et al.*, 1993).

Turbidity currents and related downslope processes have been inferred, though less commonly than alongslope thermohaline flows, as an alternative origin for relatively localized sediment wave fields found on the levees of large deep-sea channels and submarine fan valleys. The occurrence of such wave fields has been reported from the Toyama Basin (Nakajima, 1996; Nakajima *et al.*, 1998), the Tosa basin (Blum and Okamura, 1992), the Bellingshause Basin (Tucholke, 1977), the Hueneme Fan in the Santa Monica Basins (Nardin, 1983; Piper *et al.*, 1996), the Var Sedimentary Ridge (Piper and Savoye, 1993), the Magdalena Fan (Kolla *et al.*, 1984), the Ascension/Monterey levee (Hess and Normark, 1976; Normark *et al.*, 1980), the Demerara Outer Ridge (Embley and Langseth, 1977), the Bounty Channel levees (Carter *et al.*, 1990), the Amazon cone (Damuth, 1975; Damuth and Hayes, 1977), and the South China Basin (Damuth, 1979). These sediment waves typically occur on the higher levee, trend subparallel to channel axes and decrease in both amplitude and wavelength down the levee back slope. Otherwise, they are similar in shape, size and migration pattern to those produced by thermohaline flow.

These origins have been identified based on the locations of the features and on the nature of the sediments. However, a turbidity current origin could not be ruled out for some wave fields which are of a large regional extent (Jacobi *et al.*, 1975; Bouma and Treadwell, 1975; Damuth, 1979). There have been several reports indicating interaction of different kinds of flow (Asquith, 1979; Embley and Langseth, 1977; Marani *et al.*, 1993) and co-existance of sediment waves of different origin in a small area (Damuth and Hayes, 1977; Tucholke, 1977). Using the nature of sediments to identify the sediment wave origin is problematic as there are no generally accepted criteria for distinguishing between turbidites and contourites (Stow, 1979).

The term "mudwaves" has been preferred to describe large-scale wavy bedforms in the deep-sea (Flood and Shor, 1988), specifically those associated with bottom current activity. In this thesis the term "mudwaves" is used only for the sediment waves which can be clearly interpreted as being of bottom current origin. On the other hand, the term "sediment waves" can be applied to almost any relatively large scale sinusoidal topography regardless of their origin. To emphasize the possibility of other origins, the term "sediment waves" is used to describe these bedforms in this thesis.

Mechanisms for sediment wave formation

Several mechanisms have been proposed for the development of sediment waves. Some early studies suggested sediment waves could be compressional or extensional features associated with submarine mass wasting processes (Ballard, 1966; Egloff, 1972; Jacobi and Mrozowski, 1979; Lewis, 1971; Lonsdale, 1975). However, the regular shape with continuous seismic reflectors of sediment waves is inconsistent with a deformational origin, except for some examples specifically showing irregular shapes. It is now widely accepted that sediment waves are depositional and/or erosional features created by submarine flow activities.

Analogies of deep-sea sediment waves with fluvial bedforms have been inferred by several authors (Fox *et al.*, 1968; Ewing *et al.*, 1971; Bouma and Treadwell, 1975). Kolla *et al.* (1980) modeled the formation of sediment waves in the Mozambique Basin based on the mechanism of fluvial antidunes and associated internal waves. Normark *et al.* (1980) interpreted the sediment waves on the Monterey fan levees as antidunes created by turbidity currents, and estimated paleocurrent conditions using the modified relationship of antidunes. Richards *et al.* (1987) described the waves in the Rockall Trough as "deep-water climbing dunes", and interpreted them as having developed in a similar way as climbing sand ripples. As to the process of formation, however, care must be taken for such inferences considering the enormous difference in scale.

The most widely accepted model for sediment wave formation is the "lee-wave model"

suggested by Flood (1988). Lee waves are generated in a stratified flow crossing over a topographic high (Queney, 1948; Miles, 1968), and lead to preferential deposition or less erosion on the upstream flank of the wave. Flood (1988) quantified this process to determine the effects of mean flow velocity on migration patterns of sediment waves. Blumsack and Weatherly (1989) extended Flood's model to account for the tendency of the waves to be oriented obliquely to the mean flow direction. The lee wave model has been confirmed by current meter observations (Blumsack and Weatherly, 1989; Weatherly, 1993) and intensive studies on sediment waves in the Argentine Basin (Project MUDWAVES; Manley and Flood, 1993).

While the lee wave model successfully describes sediment wave formation by steady contour currents, application of the model to turbidity currents remains controversial. Piper and Savoye (1993) showed that the conditions required for lee wave formation were inconsistent with those expected from the slope gradients in the wave field on the Var sedimentary Ridge. Lee waves form only when the Froude number of the flow is less than $1/\pi$ (Yih, 1969; Allen, 1982b), whereas turbidity currents on the wave fields are assumed to be almost supercritical ($Fr > 1$). Although the possibility of a lee wave origin should not be ruled out, it is unlikely that sediment wave formation by turbidity currents and by contour currents can be modeled in the same way. The exact mechanism of sediment wave formation by turbidity currents is still unknown.

Deposition from turbidity currents

Turbidity currents are density (gravity) currents which are driven by their excess density caused by suspended particles. Dynamics of density currents have been studied intensively, both experimentally and theoretically (see reviews by Simpson, 1982, 1997). As many aspects of turbidity currents are similar to those of other types of density currents, most of the knowledge of turbidity current motion has been derived from studies on non-particulate density currents. Specifically, the motion of the head of a density surge has been intensively studied in order to establish expressions for density current propagation (Benjamin, 1968; Britter and Simpson, 1978;

Britter and Linden, 1980; Huppert, 1982; Huppert and Simpson, 1980; Middleton, 1966a, 1966b; Noh and Fernando, 1992; Rottman and Simpson, 1983; Simpson and Britter, 1979) and for mixing at the head (Hallworth *et al.*, 1993; Huppert *et al.*, 1993; Linden and Simpson, 1986; Simpson, 1986). Empirical expressions for the motion of the gravity current head are employed in several models which successfully describe in a simple way the motion of turbidity currents in flumes (Bonnecaze *et al.*, 1993, 1995; Dade *et al.*, 1994; Dade and Huppert, 1995).

Less is known about sediment deposition from turbidity currents than about their hydraulics. Depositional processes of turbidity currents have been described by Bouma (1962) who interpreted the sequence of sedimentary structures in turbidite beds as evidence for deposition from a decelerating flow. This simple model has been successful in accounting for many features of ancient turbidites, though it is now clear that a better understanding is required to account for the diversity of turbidite systems (Kneller, 1995; Shanmugam, 1997). Deposition from decelerating turbidity currents has been quantified using the suspension criterion (Bowen *et al.*, 1984; Komar, 1985; Reynolds, 1987; Van Tassel, 1981) or the threshold of sediment motion (McCave and Swift, 1976; Stow and Bowen, 1980) to estimate paleocurrent conditions from turbidites. Hiscott (1994) suggested that loss of capacity should be the fundamental process governing deposition from turbidity currents.

There has been a number of experimental studies on sediment deposition from turbidity currents looking at both a two-dimensional deposition pattern (e.g. Middleton, 1967) and a three-dimensional pattern (e.g. Lüthi, 1981). It has generally been observed that the thickness of the deposit decreases downstream (Middleton, 1967; Middleton and Neal, 1989; Laval *et al.*, 1988). Recent studies have reported that the deposit distribution exhibits a peak somewhat downstream of the gate (Bonnecaze *et al.*, 1993, 1995; Gladstone *et al.*, 1998). The experimental study of Gladstone *et al.* (1998) showed a systematic variation in profiles of the deposit distribution with particle size, even though the peak position was independent of particle size. It is thought that the deposit distribution is determined by two factors in the temporally evolving current: the

diminishing rates of deposition and current velocity at a fixed point along the travel path (Dade and Huppert, 1995).

While most experimental studies of turbidity currents and turbidites have concentrated on unidirectional flow on a flat surface or on a constant slope, several studies investigated topographic effects on deposition from turbidity currents. The reflection of density currents has been studied (Pantin and Leeder, 1987; Edwards, 1993; Kneller *et al.*, 1991) to simulate sediment ponding and reversals of paleocurrent direction observed in natural turbidite systems (Hersey, 1965; van Andel and Komar, 1969; Hieke, 1984; Cita *et al.*, 1984; Lebreiro *et al.*, 1997; Ricci Lucci and Valmori, 1980; Pickering and Hiscott, 1985; Marjanac, 1990). However, there are only a few studies on topographic effects on turbidite deposition other than reflection (Siegenthaler *et al.*, 1984; Muck and Underwood, 1990; Alexander and Morris, 1994). No attempts have been made in a laboratory to simulate turbidite deposition on a wavy bed, or to relate the topographic effects to the development of undulation in turbidites.

There is an increasing number of studies on numerical modeling of turbidity currents. Two end-members can be classified: (1) those using the Navier-Stokes flux equations and (2) those using force equilibrium according to Newton's second law. Force equilibrium models include those using a Chézy type equation, which represents steady flow conditions and is derived from the balance between gravity and the force due to fluid resistance. The Chézy equation has been verified by experimental studies (e.g. Middleton, 1966b), and is employed by many authors to predict theoretically the motion of turbidity currents both in laboratory flumes and in nature (Kersey and Hsü, 1976; Komar, 1970; 1971; 1972; 1973; van Tassel, 1981; Chikita, 1990; Hay, 1983; Reynolds, 1987; Kostaschuk *et al.*, 1992; Piper and Savoye, 1993; Piper *et al.*, 1988). Surge-type turbidity currents have been modeled as a non-steady propagation of a suspension cloud (Beghin *et al.*, 1981; Kirwan *et al.*, 1986; Dade *et al.*, 1994; Mulder *et al.*, 1998).

Flux models of turbidity currents are often represented by one-dimensional solutions of equations for conservation of momentum, water and sediments (Ellison and Turner, 1959; Pantin,

1979; Parker, 1982). Several models include empirical relationships for sediment transport and friction slope (Fukushima *et al.*, 1985; Zeng and Lowe, 1997a) and turbulent kinetic energy (Parker *et al.*, 1986). Although some models employed full descriptions of vertical structures of the flow (Akiyama and Stefan, 1984; Stacey and Bowen, 1988, Eidsvik and Brørs, 1989), more simple layer-averaged equations have been more commonly employed (Buehler and Siegenthaler, 1986; Chu *et al.*, 1984; Parker, 1982; Parker *et al*, 1986; Fukushima *et al.*, 1985; Zeng and Lowe, 1997a).

Some recent studies attempted numerical simulation of natural turbidity currents in specific areas (Zeng and Lowe, 1997a, 1997b; Mulder *et al.*, 1998; Kirwan *et al.*, 1986; Dade and Huppert, 1994). These studies are more or less successful as case studies of reconstruction of the relationship between a turbidite bed and the turbidity current. However, no attempt has been made to investigate accumulation patterns of a large number of turbidite beds.

In the following two sections, the patterns of turbidite deposition are studied both by laboratory experiments and by numerical calculations, to simulate the sediment wave formation by overspill turbidity currents on abyssal levees.

3.2 Laboratory experiments

3.2.1 Experimental procedures

Experiments were carried out in order to investigate the spatial distribution of turbidity current deposits. The experiments were performed at Osaka University (Department of Earth and Space Science), using a laboratory flume 10 m long, 20 cm wide and 50 cm deep (Fig. 3.1). For the turbidity current experiments, the flume was modified by the insertion of a gate box at the upstream end. The box was built with 1 cm thick acrylic boards, and had inside plan dimensions of 50 cm long and 17 cm wide. The bottom inside the box was 1 cm above the bottom of the flume due to the

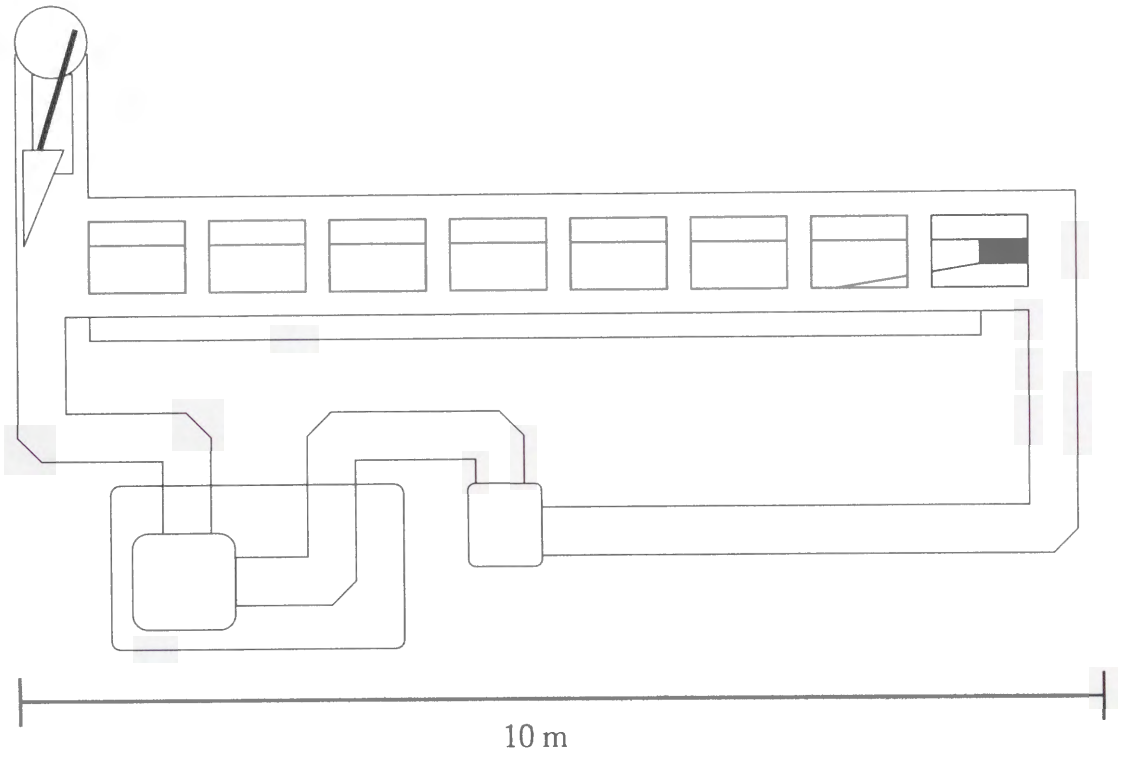

Fig. 3.1. Illustration of the flume in Osaka University. The flume is 10 m long, 20 cm wide and 50 cm deep.

thickness of the board, but the step was canceled by placing the same boards on the flume floor. One end of the box could be slid up and down to act as a gate to release heavier fluid within the box. The lock exchange is a common method to produce density currents in laboratory experiments (Huppert and Simpson, 1980; Beghin *et al.*, 1981; Rottman and Simpson, 1983; Laval *et al.*, 1988; Edwards, 1993; Bonnecaze *et al.*, 1993, 1995; Gladstone *et al.*, 1998; see Middleton, 1993 for review).

A turbidity current was generated by releasing a suspension, which was made by mixing siliceous, non-cohesive particles of varying diameter. The settling velocities of the particles measured in a settling tube system in Osaka University showed a modal value of 0.9 cm/s, corresponding to 3.2 ϕ in grain size, and the median value of 0.6 cm/s, corresponding to 3.5 ϕ in grain size. The settling velocity distribution of the particles is shown in Fig. 3.2, together with corresponding grain size estimated from Gibbs' formula (Gibbs *et al.*, 1971) using a representative value of 2.65 g/cm^3 for the density of siliceous particles. The initial volume fraction of particles in suspension was set between 1.0 - 3.3% in each run. The range of the volume fraction is sufficiently lower than the value above which grain to grain interaction is possibly effective (e.g. 9%; Middleton and Southard, 1984; Sanders, 1965). The initial density of the suspension, ρ_0, with volume fraction, C, is given by

$$\rho_0 = (\rho_p - \rho_w) C + \rho_w$$

where ρ_p and ρ_w are the densities of the particles and the ambient water, respectively. The excess density of the turbidity current, $\Delta\rho$, is equal to 1.65 C.

The particles were added to the fluid in the box until the required volume fraction was reached, and stirred in the box by hand. After full particle suspension was ensured, 2 sec was allowed before current initiation in order to reduce the turbulence level of the suspension. The gate was then smoothly lifted above the water surface to release the suspension into the main channel. The suspension formed an underflow (Fig. 3.3) until it dissipated. In several runs, the current reached the endwall of the flume, but no significant reflection of the current was observed.

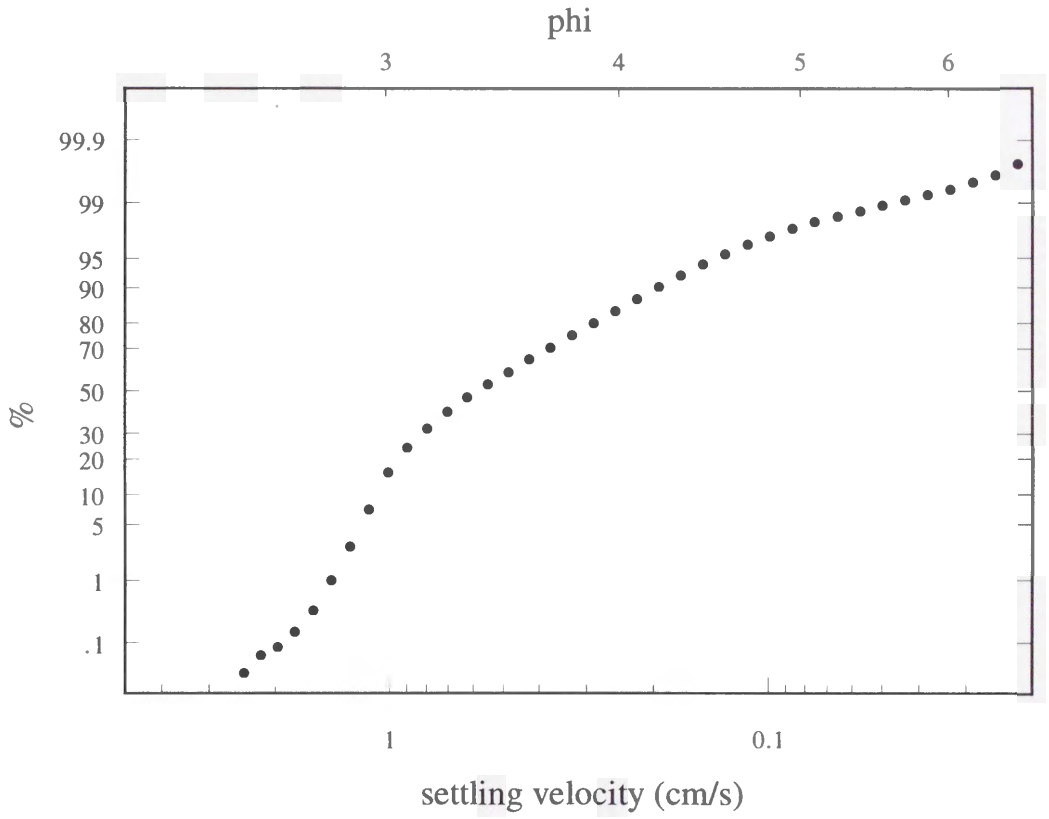

Fig. 3.2. Settling velocity distribution of sediments used in the experiments. The modal value of the settling velocity is 0.9 cm/s, corresponding to a grain size of 3.2 ϕ, and the median value is 0.6 cm/s, corresponding to a grain size of 3.5 ϕ.

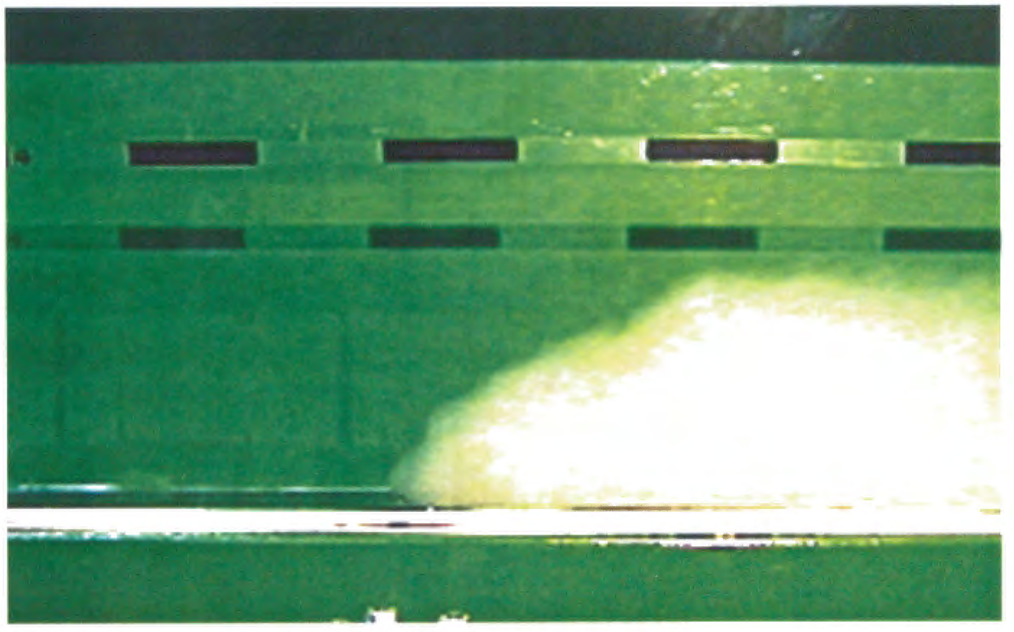

Fig. 3.3. Picture of a turbidity current head in the laboratory experiment. Flow is from right to left. Scales (black bars) are 10 cm.

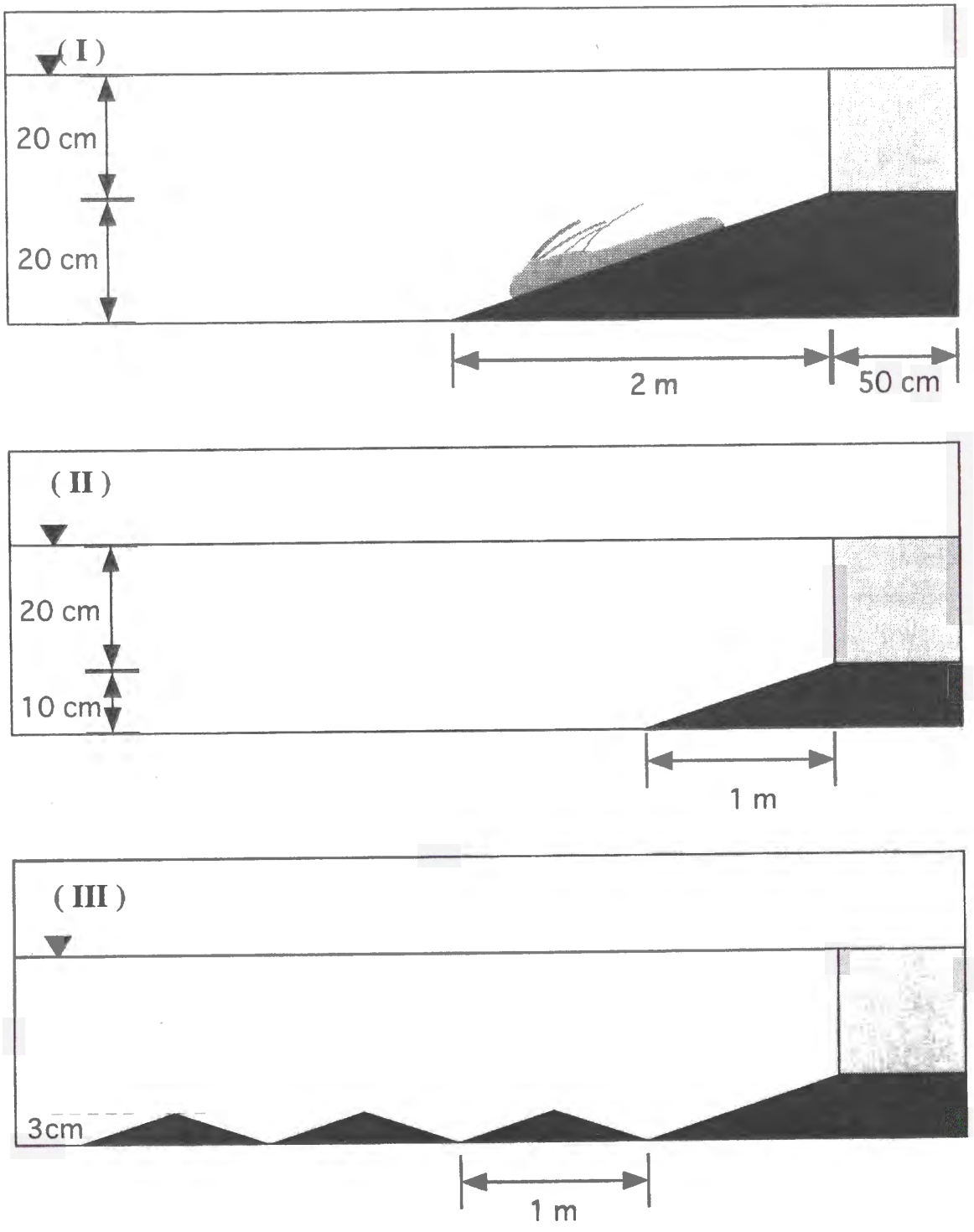

Fig. 3.4. Illustration of the "flat slope" topography (I & II) and "zig-zag" topography (III) in the experiments. The flat slope topography starts with 1/10 slope and then becomes flat. The horizontal lengths of the slope are 2 m (I) and 1 m (II). The zigzag topography includes three ups and downs after a slope of 1/10 for 1 m. Each up and down is 3 cm high and 50 cm long. The gate box is 50 cm long and placed in the flume horizontally. The shorter gate box (25 cm) is used in B4 and B8. The water depth in the gate box is 20 cm.

After the particles had been deposited, the volume of the deposit on a fixed area was measured along the length of the flume. A stainless steel cylinder with an internal diameter of 4 cm was centered on the resultant deposit on the bottom of the flume at specific locations (10 - 50 cm intervals) along the flume, and all the particles within the cylinder were removed by a siphon tube. The particles collected were dried and then weighed to determine the "deposit density" (mass per unit bed area; Gladstone *et al.*, 1998) profile along the flume.

Three series of runs were carried out. The runs in the first series (Run A1 - A6) were preliminary runs to check the reliability of the experimental procedures. The flume was set horizontally and filled to a height of 40 cm with tap water. The initial volume fractions were 1.1% in Runs A1 and A2, 2.2% in Runs A3 and A4 and 3.3% in Runs A5 and A6. Other conditions were the same throughout these 6 runs. Apart from the siphon method, a different particle collection method was used in run A4. Plastic sheets were placed in advance between sampling locations for the siphon tube method in Run A4. Particles on the sheets were collected after the water had been drained off from the flume. This method was performed to be compared with the siphon tube method.

The second and third series were performed to investigate topographic effects on deposition by turbidity currents. The second series on a "flat slope" topography (Fig. 3.4) comprised eight runs with different conditions. The bed was tilted to a degree of 1/10 from the gate, and was then flat to the downstream end. In the first four runs (B1 - B4) the slope ended at 2 m from the gate and in the next four runs (B5 - B8) the slope ended at 1 m. The gate box was placed horizontally 20 cm above the bed in B1 - B4 and 10 cm in B5 - B8. The water depth was kept at 20 cm in the gate box through all runs in the second series, i.e., 40 cm and 30 cm from the bottom of the flume in runs B1 - B4 and runs B5 - B8, respectively.

Initial volume fraction of the particles was 2%, except for runs B2 and B6 in which the volume fraction was reduced to 1%. In runs B3 and B7, the suspension was made with finer particles, which were taken by sieving the original particles with a 3.5 ϕ mesh. In runs B4 and B8, the length

of the gate box was shortened to 25 cm to check the effects of the back wall.

For the two flows of the third series a "zig-zag" topography (Fig. 3.4) of three ups and downs was added to the "flat slope" topography of runs B5 - B8 (1 m slope). Each up and down was 3 cm high and 50 cm long. Otherwise the conditions in C1 were the same as in run B5, while the finer particles used in runs B3 and B7 were again employed in C2.

3.2.2 Results

First series

The measured deposit density in each run is plotted in Fig. 3.5. The deposit density profiles show a monotonous decrease with distance for the flat channel, except for A6 (Fig. 3.5). The good agreement between A1 and A2 and between A3 and A4 confirms the reliability of the methods. The two plots of A4, representing different methods in collecting the particles, show a fairly smooth profile, confirming the accuracy of the siphon tube technique. The plots of A5 and A6, however, show considerable differences, which are considered to be a consequence of the higher suspension concentration (3.3%). To avoid this uncertainty, the volume fraction of suspension was set at either 1.0 or 2.0% in the following series.

Second Series

The results of B1 and B5 are plotted in Fig. 3.6 to show the topographic effects on the deposit density. As the same currents are formed to flow down the slope in these runs, the deposit densities show good agreement with each other until 1 m from the gate, where the slope break is encountered in B5. In both runs, the deposit densities decrease from a maximum at the most proximal sampling points, then exhibit a peak at 0.8 - 1 m downstream of the slope break. The results of the short-slope run (B5) shows a distinctive peak at 80 cm downstream of the slope break, while the long-slope run (B1) shows a slight increase within 1 m from the slope break.

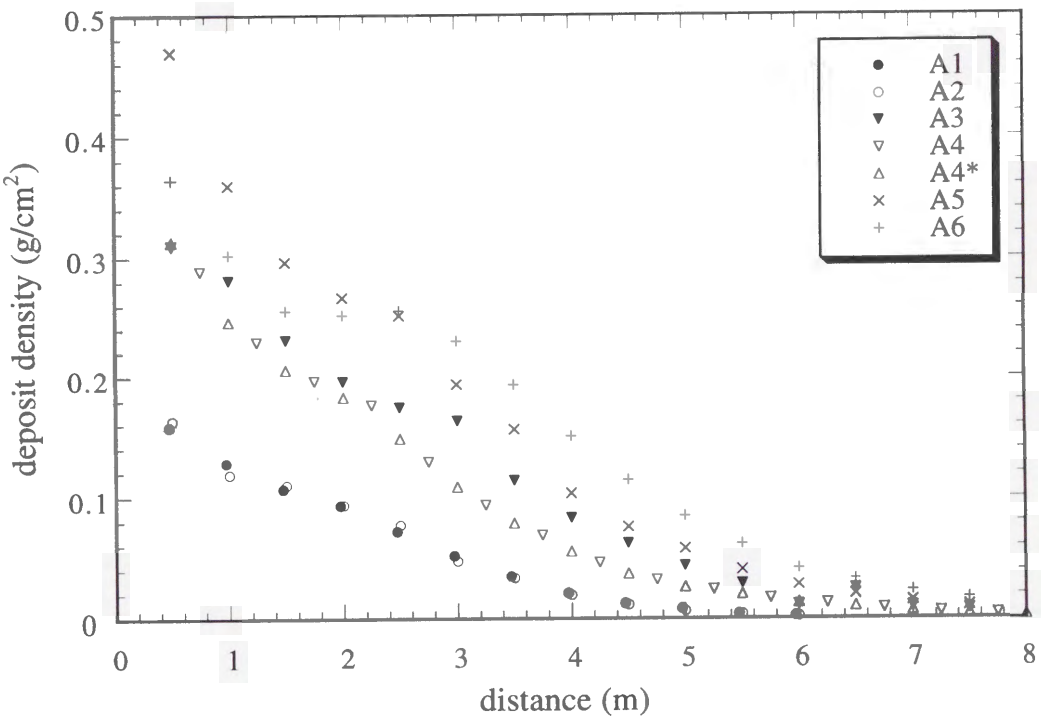

Fig. 3.5. The deposit density profiles on the flat bed. The sediment concentration is 1.1% in A1 and A2, 2.2% in A3 and A4, and 3.3% in A5 and A6. Samples were collected by siphon tube method except for A4* in which samples were collected using plastic sheets.

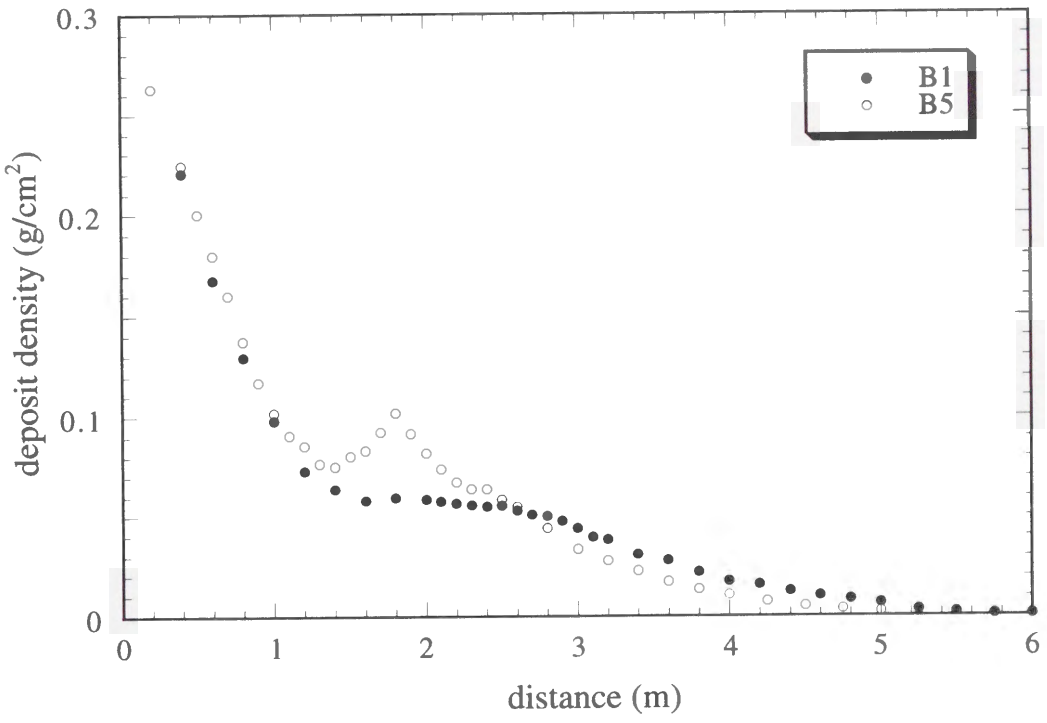

Fig. 3.6. The deposit density profiles on the flat slope topography. The horizontal length of the slope is 2 m in B1 and 1 m in B5.

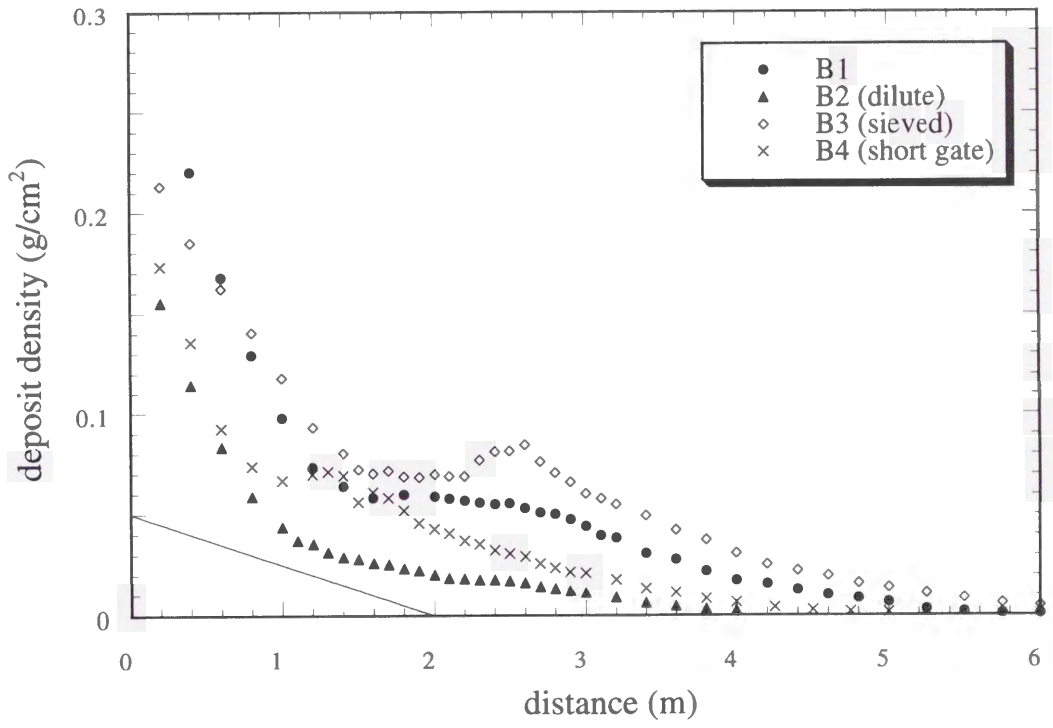

Fig. 3.7. The deposit density profiles on the flat slope topography with a 2 m slope. Compared to B1, the flow is dilute (1%) in B2, finer particles (sieved with 3.5 ϕ mesh) are used in B3, and the shorter gate box (25 cm long) is used in B4. Otherwise the conditions are the same as in B1.

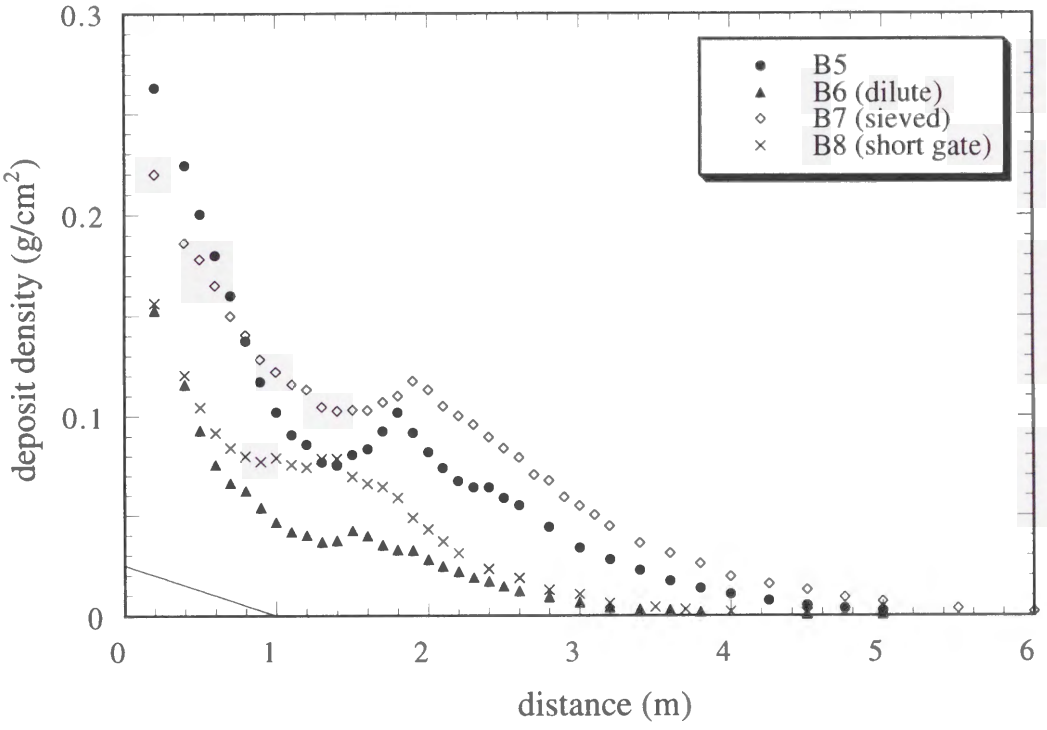

Fig. 3.8. The deposit density profiles on the flat slope topography with a 1 m slope. Compared to B5, the flow is dilute (1%) in B6, finer particles (sieved with 3.5 ϕ mesh) are used in B7, and the shorter gate box (25 cm long) is used in B8. Otherwise the conditions are the same as in B5.

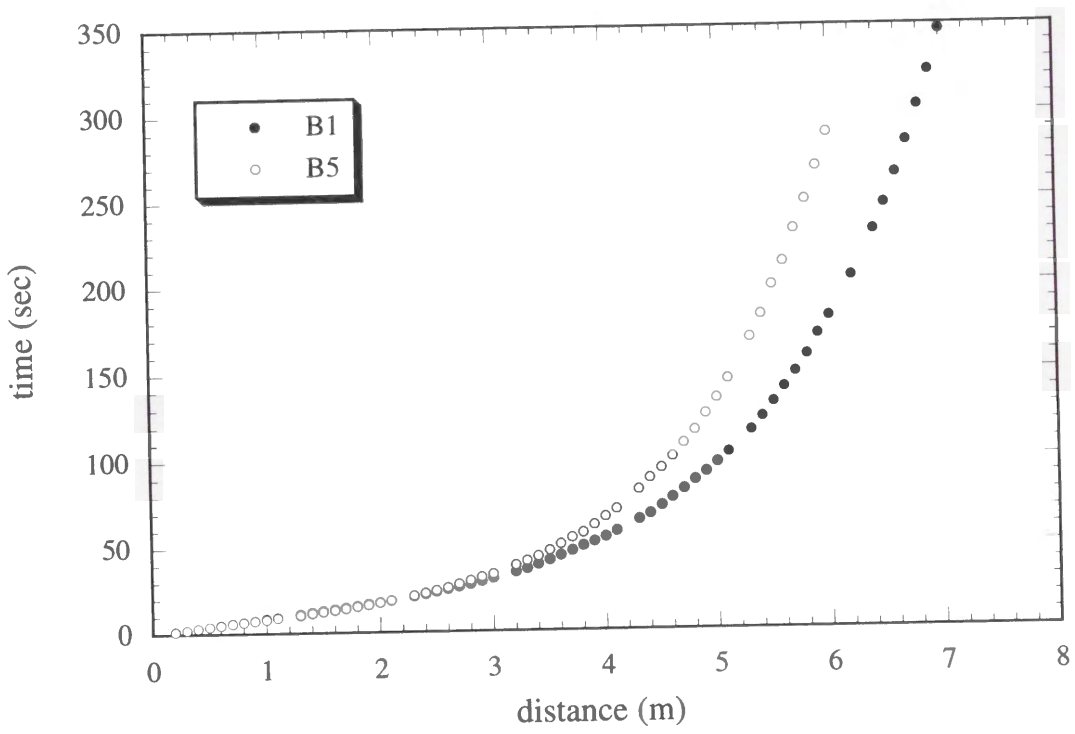

Fig. 3.9. The relationship between time and travel distance of the flow head. The flow in B5 is slower than in B1 due to the shorter slope.

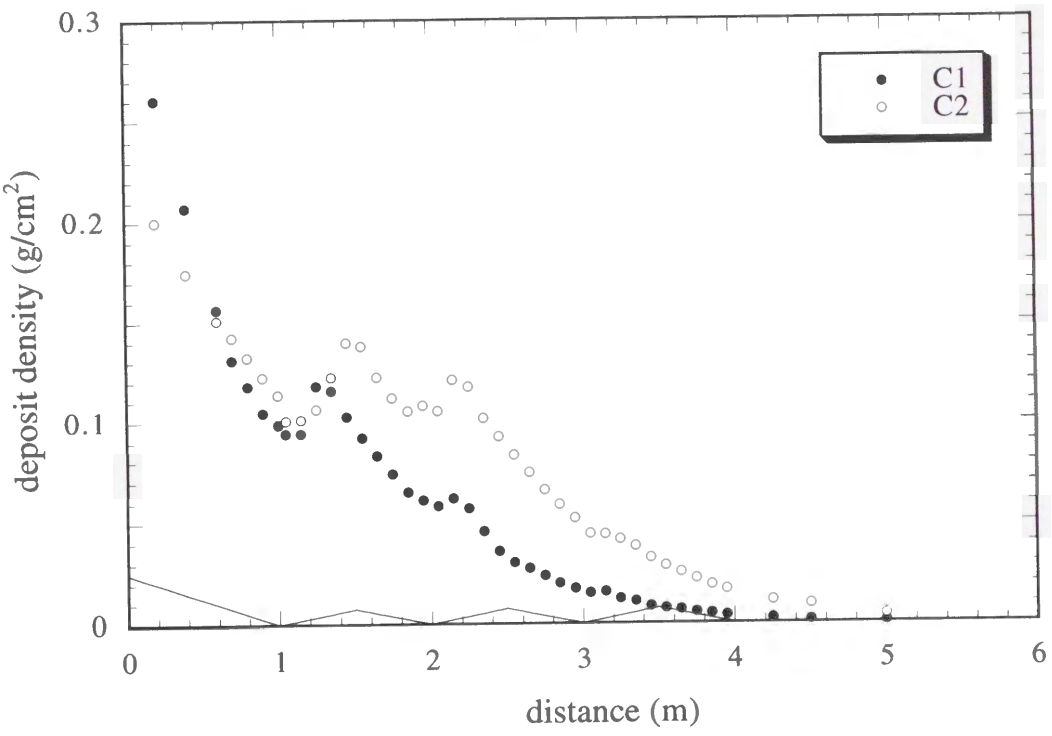

Fig. 3.10. The deposit density profiles on the zig-zag topography. Compared to C1, finer particles (sieved with 3.5 ϕ mesh) are used in C2. Otherwise the conditions are the same.

The variation of the deposit density profile with different initial conditions is shown in Fig. 3.7 and Fig. 3.8. The plots for the lower concentration flows (B2 and B6) both show less distinctive peaks, while the plots for the finer particle flows (B3 and B7) show distinctive peaks and more transport of particles downstream. There is no systematic variation in the position of the peaks in these runs (B1 - B3, B5 - B7). The position of the peak shifts upstream in the plots for the shorter box-length (B4 and B8), though the peaks are not very distinctive.

The travel distance with time of the head from the gate is plotted in Fig. 3.9. The flows in B1 and B5 both travel the first 1 m in about 10 sec. The flow in B5 decelerates earlier than the flow in B1 due to the shorter slope, though there is no sudden deceleration at the slope break. The flow in B1 travels 6 meters in 180 sec, and the flow in B5 takes 287 sec to travel this distance.

Third series

The deposit density profiles of C1 and C2 are plotted in Fig. 3.10, both showing distinctive peaks on every upslope. The plot for the flow with finer particles (C2) shows more transport of particles to the downstream area, which can also be seen for these flows in the second series (B3 and B7).

3.2.3 Discussion

The results of the second series imply that a mound is formed by deposition from a turbidity current encountering an appropriate slope break. The mound is developed provided that such turbidite deposition is repeated, resulting in a new slope break on the lee-side downslope of the mound.

A peak in the deposit density profile has been found in experiments on a flat surface (Bonnecaze *et al.*, 1993; Gladstone *et al.*, 1998). The peak is considered to result from two competing factors in the temporally evolving current: the diminishing rates of deposition and current

velocity at a fixed point along the travel path (Dade and Huppert, 1995). However, comparison of the results of B1 and B5 confirms that the peak in the profile of B5 is a consequence of the slope break, because these two runs produce the same current conditions on the same topography, except for the position of the slope break.

The results of the third series are directly comparable to turbidite deposition on wavy topography in natural settings. The peak in the deposit density profiles on every upslope leads to possible upstream migration of the waveform, as observed in sediment waves. The results imply that, once the wavy topography is developed, accumulation of turbidites results in the upstream migration of the waveform even without specific phenomena such as lee waves and phase equivalence in a supercritical flow.

There are scaling problems in applying the results of laboratory experiments to natural large-scale turbidity currents. The ratio of sediment size to turbidity current size in laboratory is much larger than that in nature. Middleton (1993) suggested that the settling velocity should be reduced in the experimental model by a factor of 10 to 100. The use of fine sand with the settling velocity of 0.6 cm/s in laboratory experiments means modeling of deposition of coarse sand or gravels with the settling velocity of 6 - 60 cm/s. The results of the laboratory experiments should not be interpreted as a scale-model of turbidite deposition on sediment waves which usually consist of fine sand and silt.

In all cases, on the other hand, the deposit density profiles show more distinctive peaks in the experiments using finer particles. This tendency implies that the topographic effects are more sensitively reflected in deposition from natural large scale turbidity currents, in which the size difference is much larger than that in experiments. The peaks in deposit profiles downstream of the slope break can possibly be formed in natural turbidite beds, and result in bed undulation.

At the slope break in the flume, the turbidity current should pass through a hydraulic jump. Komar (1971) showed that the slope for a turbidity current being critical ($Fr = 1$) is 0.0075, based on the formula

$$Fr = \sqrt{\frac{S}{C_d(1+\alpha)}}$$

where S ($\cong \sin\beta$) is the slope, C_d is the drag coefficient and α is the term representing relative importance of the interface and bottom drag. The topography in the flume includes slope of 0.1 (second series) or 0.06 (third series), on which a turbidity current should be supercritical.

A hydraulic jump, however, was not observed visually in all runs, at least not in a stable form. While the flow seemed more turbulent at the slope break, changes in flow velocities and flow depths were not clear enough to identify the occurrence of a hydraulic jump, because the flows were short-lived and had an ambiguous boundary with the ambient fluid. It is therefore not clear whether a hydraulic jump is responsible for the peaks in the deposit density profiles.

3.3 Numerical simulation

3.3.1 Theory

This study employs a layer-averaged three-equation model in which equations for conservation of fluid mass, sediment mass and fluid momentum are solved simultaneously. This type of model has been widely used by many authors (e.g., Chu *et al.*, 1979; Parker *et al.*, 1986; Zeng and Lowe, 1997a), and takes topographic effects into consideration and has the advantage of being less expensive computationally than a fully two-dimensional model. The layer-averaged, three-equation flow model is of the following form (Chu *et al.*, 1979; Parker *et al.*, 1986; Zeng and Lowe, 1997a):

conservation of fluid mass

$$\frac{\partial h}{\partial t} + \frac{\partial}{\partial x}(uh) = E_w u \tag{3.1}$$

conservation of momentum

$$\frac{\partial}{\partial t}(uh)+\frac{\partial}{\partial x}\left(u^2h\right)=-\frac{(\rho_s-\rho_w)g}{2\rho_w}\frac{\partial}{\partial x}\left(Ch^2\right)+\frac{(\rho_s-\rho_w)ghCS}{\rho_w}-C_d(1+\alpha)u^2 \qquad (3.2)$$

conservation of sediment mass

$$\frac{\partial}{\partial t}(Ch)+\frac{\partial}{\partial x}(uCh)=-F_d+F_e \qquad (3.3)$$

where u is the flow velocity, h is the flow thickness, g is the acceleration due to gravity, E_w is water entrainment coefficient, ρ_s and ρ_w are the densities of the sediment and water respectively, C is the volume concentration of sediments, S is the bottom slope, C_d is the drag coefficient which has a value of 0.0035-0.005 (Komar, 1971; 1985), α is the ratio of the drag force at the upper flow surface to that at the bed, and F_d and F_e are the flux of sediment deposition and erosion, respectively. Although the value of α varies with the Froude number (Middleton, 1966b), a representative constant value of 0.43 is used here (e.g. Komar, 1969; Middleton, 1966c).

Introducing non-dimensional quantities $X=x/x_0$, $U=u/u_0$ and $T=t/t_0$, and assuming a volume-conserving flow ($E_w=0$), yields for eqs. (3.1) - (3.3):

$$\frac{\partial H}{\partial T}+\frac{\partial}{\partial X}(UH)=0 \qquad (3.4)$$

$$\frac{\partial U}{\partial T}+U\frac{\partial U}{\partial X}=-\frac{R}{2}\frac{\partial}{\partial X}(CH)-\frac{R}{2}\frac{\partial H}{\partial X}+RCS-C_d(1+\alpha)U^2/H \qquad (3.5)$$

$$\frac{\partial CH}{\partial T}+\frac{\partial}{\partial X}(UCH)=\left(-F_d+F_e\right)/u_0 \qquad (3.6)$$

where $H=h/x_0$, $R=(\rho_s-\rho_w)/\rho_w$, $u_0=(gx_0)^{1/2}$, $t_0=(x_0/g)^{1/2}$, and x_0 is the length of the cells in the numerical calculations.

Erosion and deposition of particles

The sediment flux at the bed is determined from the rates of deposition (F_d) and erosion (F_e). The rate of deposition, F_d, is described as the product of the settling velocity of sediment, w_s, and the fractional concentrations of suspension at the bed, C_b. For multiple grain sizes, the sum of this

product for each size population is used as the net rate of deposition.

The sediment concentration at the bed, C_b, has often been approximated from the average concentration, C, using a Roussean-type expression (Parker, 1982; Parker *et al.*, 1986; Fukushima *et al.*, 1985; Zeng and Lowe, 1997a) as

$$C_b/C = 1+31.5\ (u_*/w_s)^{-1.46}$$

This formula has been tested for a laboratory turbidity current and showed good agreement for the range $5 < u_*/w_s < 50$ (Parker *et al.*, 1986). This range represents a flow velocity range of 35 cm/s $< u <$ 8.5 m/s with a settling velocity of 0.5 - 1 cm/s and a drag coefficient of 0.0035 - 0.005. In laboratory experiments in this study, however, the flow velocity of turbidity currents was usually less than 35 cm/s. In large-scale turbidity currents in nature, even though the flow velocity is within the appropriate range, the particle distribution is unlikely to be in the equilibrium condition of a Roussean-type distribution. It is expected that there is a considerable time-lag before slow-moving particles attain an equilibrium distribution adapting to varying flow conditions. Therefore the value of C_b is arbitrarily assumed to be equal to the average concentration, C, in this model.

In order to describe the sediment entrainment from the bed, Fukushima *et al.* (1985) used a dimensionless number, Z, determined as

$$Z = \left(\frac{\sqrt{RgD_s}D_s}{\nu} \right)^{1/2} \frac{u_*}{w_s}$$

where D_s is the diameter of the particle, and ν is the kinematic viscosity of water. The rate of sediment entrainment, F_e, is described as $w_s E_s$ with,

$$E_s = \begin{cases} 0 & Z < 5 \\ 3 \times 10^{-12} Z^{10} \left(1 - \dfrac{5}{Z}\right) & 5 < Z < 13.2 \\ 0.3 & 13.2 < Z \end{cases} \qquad (3.7)$$

Though often used for turbidity current modeling in nature (Zeng and Lowe, 1997a; Fukushima *et al.*, 1985), Eq.(3.7) is based on an empirical expression for sand-sized sediments. It

should be noted that the bed surface on submarine levees is covered with pelagic material, which consists of silt- or clay-sized sediment that is easily consolidated. In order to describe the erosion of the deep-sea floor by turbidity currents, Mulder *et al.* (1998) assumed that erosion occurs if the shear stress created at the bottom of the flow, τ_b, exceeds the shear resistance of the sea bottom sediment, τ_s, using the quadratic stress law

$$\tau_b = C_d \rho_f u^2$$

and the relationship in which τ_s depends on the depth z,

$$\tau_s = a z + b$$

Assuming that the maximum depth value for erosion, $z = (C_d \rho_f u^2 - b)/a$, occurs over one day, the rate of erosion (in m/s) is determined as

$$F_e = (C_d \rho_f u^2 - b)/(a\, 86400) \tag{3.8}$$

This erosion equation is sensitive to the values of a and b which must therefore be carefully calibrated by measurements. In this study, it is assumed that a =3.5 and b =0.2 based on the measurements of the shear strength of the marine sediment of the Saguenay Fjord (Mulder *et al.*, 1998).

This study uses eq. (3.7) for modeling of turbidity currents in laboratory experiments, in which sand-sized sediment was used, and eq. (3.8) for simulating submarine turbidity currents.

3.3.2 Computation

A computer algorithm is written in Mathematica™ to calculate the evolution of turbidity currents. The flow system is represented by space-fixed cells at which flow properties are evaluated. The temporal evolution of the field properties of the flow is computed from eqs. (3.4) - (3.6) with the aid of eq. (3.7) or (3.8). The computation employs staggered cells, in which the flow velocity (U) is calculated at the boundary of each cell while the flow depth (H) and the sediment concentration (C) are calculated at the center of the cell (Fig. 3.11). The advantages of this

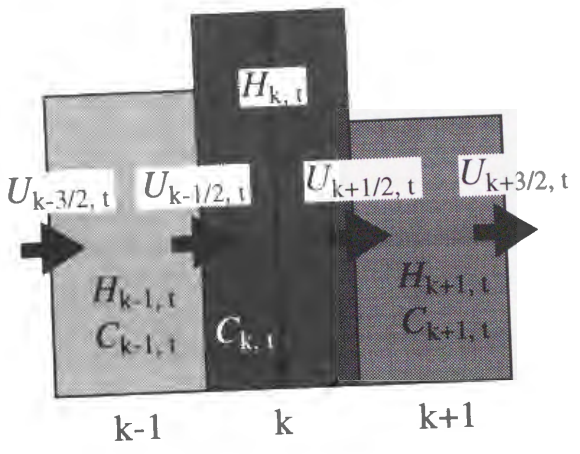

Fig.3.11. Staggered cell employed in the numerical model. The flow velocity (U) is calculated at the boundary of each cell while the flow depth (H) and the sediment concentration (C) are calculated at the center of the cell. The flow velocity (U) is calculated at the boundary of each cell while the flow depth (H) and the sediment concentration (C) are calculated at the center of the cell.

method are ease of discretization and conservation of mass in every cell.

For given $U_{k+1/2,t}$, the flow velocity at cell k is updated using the first-order accurate Euler-forward method as,

$$U_{k+1/2,t+1} = U_{k+1/2,t} + \Delta T\left(\frac{\partial U}{\partial T}\right)_{k+1/2,t}$$

where ∂ T is the time increment and ∂ U/∂ T is determined from eq. (3.5) as

$$\left(\frac{\partial U}{\partial T}\right)_{k+1/2,t} = -U_{k+1/2,t}\left(\frac{\partial U}{\partial X}\right)_{k+1/2,t} - \frac{R}{2}\left(\frac{\partial CH}{\partial X}\right)_{k+1/2,t} - \frac{R}{2}\left(\frac{\partial H}{\partial X}\right)_{k+1/2,t} + R(CS)_{k+1/2,t} - C_{\mathrm{d}}\left(\frac{U^2}{H}\right)_{k+1/2,t}$$

In the first term on the right hand side of this equation, the gradient of the flow velocity is calculated using a first-order upwind difference scheme

$$\left(\frac{\partial U}{\partial X}\right)_{k+1/2,t} = \begin{cases} U_{k+1/2,t} - U_{k-1/2,t} & for \quad U_{k+1/2,t} \geq 0 \\ U_{k+3/2,t} - U_{k+1/2,t} & for \quad U_{k+1/2,t} < 0 \end{cases}$$

The upwind difference scheme is employed to avoid numerical oscillation caused by the central difference scheme. The second to fourth terms are written simply as

$$\left(\frac{\partial CH}{\partial X}\right)_{k+1/2,t} = C_{k+1,t}H_{k+1,t} - C_{k,t}H_{k,t}$$

$$\left(\frac{\partial H}{\partial X}\right)_{k+1/2,t} = H_{k+1,t} - H_{k,t}$$

$$(CS)_{k+1/2,t} = C_{k+1,t}Z_{k+1,t} - C_{k,t}Z_{k,t}$$

where Z is the bed topography. The final term is calculated from

$$H_{k+1/2,t} = \begin{cases} H_{k+1,t} & for \quad U_{k+1/2,t} \geq 0 \\ H_{k,t} & for \quad U_{k+1/2,t} < 0 \end{cases}$$

From eqs. (3.4) and (3.6), the flow depth and the sediment concentration are updated as,

$$H_{k,t+1} = H_{k,t} + \Delta T\left(\frac{\partial H}{\partial T}\right)_{k,t}$$
$$= H_{k,t} + \Delta T\left(-U_{k+1/2,t+1}H_{k+1/2,t} + U_{k-1/2,t+1}H_{k-1/2,t}\right)_{k,t}$$

$$C_{k,t+1} = \frac{1}{H_{k,t+1}}\left(C_{k,t}H_{k,t} + \Delta T\left(\frac{\partial CH}{\partial T}\right)_{k,t}\right)$$
$$= \frac{1}{H_{k,t+1}}(C_{k,t}H_{k,t} + \Delta T(-U_{k+1/2,t+1}C_{k+1/2,t}H_{k+1/2,t}$$
$$+ U_{k-1/2,t+1}C_{k-1/2,t}H_{k-1/2,t} - W_s(C_{k,t} - E)))$$

where the boundary values for C and H are determined as

$$C, H_{k+1/2} = \begin{cases} C, H_k & for \quad U_{k+1/2} \geq 0 \\ C, H_{k+1} & for \quad U_{k+1/2} < 0 \end{cases}$$

The amount of deposited/eroded sediment is calculated from the sediment flux at the bed, and converted to bed thickness by assuming sediment porosity to be 0.5. Effects of post-depositional compaction are ignored.

The time step was chosen considering the Courant-Friedrichs-Levy condition, i.e., not to exceed the minimum value of the grid interval divided by the flow velocity. The calculation is continued until the maximum concentration is below 1% of the initial value.

Model input for simulation of the laboratory experiments

The initial and boundary conditions required in the model calculations are given so as to be consistent with the corresponding flume experiments. The flow field in the 8 m long flume is represented by 400 cells at 2 cm intervals. The settling velocity and the diameter of the particles are represented by three components; 40% of the fraction representing fine sand (w_s =1.0 cm/s, ϕ =3.0), 50% of very fine sand (w_s =0.6 cm/s, ϕ =3.2) and 10% of silt-sized sediments (w_s =0.2 cm/s, ϕ =4.5). The sieved particles used in runs B3 and B7 are represented by a 7:3 mixture of the

very fine sand and the silt-sized fractions.

Model input for simulation of natural settings

The conditions to most likely simulate spillover turbidity currents on submarine channel levees are used. The flow field of 20 km long is represented by 200 cells at 100 m intervals. A model turbidity current is generated by supplying a stationary suspension at the upstream end (top of the levee) of the system. The stationary suspension is modeled by fixing the boundary conditions of the particle concentration and the height of suspension for a given supply duration. The initial concentration is set at 0.1% ($\Delta\rho$ =1.65 10^{-3} g/cm^3) or 0.5% ($\Delta\rho$ =8.25 10^{-3} g/cm^3), sufficiently less than the values used in calculations of the main head/body of the turbidity current flowing in a channel (cf. 3 - 12% by van Andel and Komar, 1969; 5 - 10% by Komar, 1969; ρ =1.2 g/cm^3 by Komar, 1973; 6% by Hiscott, 1994, 1 - 25% by Zeng and Lowe, 1997a) and comparable to those estimated for spillover turbidity currents from fan deposits (0.01 - 0.2% by Bowen *et al.*, 1984). The initial height of the suspension is set at 20 or 50 m so as to be (i) of the same order as but less than the typical values of observed heights of submarine channels which are accompanied by levees, and (ii) comparable to the difference of heights of the levees on opposite sides of the channel (Normark *et al.*, 1980, Komar, 1969). The supply duration is set at 20 or 60 min, which is comparable to the passage time of a surge type flow estimated from the deposition rate (20 - 52 min by Allen, 1991). The particles are represented by a single grain size whose settling velocity is 0.3 or 1.0 cm/s. A constant slope less than 1/100 is assumed as initial topography.

In simulating sediment wave formation, the deposition from turbidity currents is repeated for multiple flow events. The volume of deposits is converted to thickness by assuming the sediment porosity to be 0.5. As the deposition thickness is small (<0.1 m) compared to the scale of the system, the thickness of a single turbidite bed is amplified 10 times and then added to the bed topography. The amplification assumes that the change of topography by a single turbidite bed has so little influence on the next deposition that the same thickness profiles can be used for 10 turbidite

beds. Post-depositional compaction and pelagic sedimentation are ignored because they affect thickness in an almost uniform way and have no influence on the development of the wavy structures, even though the thickness of the deposits is varied.

3.3.3 Results

Comparison with the laboratory experiments

The results of the numerical calculations are plotted in Figs. 3.12 - 3.20 and are compared with the results of experiments.

First series: In the flat-bed case, the model predicts monotonous decreases in the deposit densities with distance from the gate (Fig. 3.12). The gradient of the decrease, as well as the total amount of the deposits, increases with higher initial values for particle concentration in suspension. The comparison with experiments shows good agreement, except for the high-concentration runs (A5 and A6), which show a lot of fluctuation.

Second series: Figures 3.13 and 3.14 show the model predictions for the deposit density profiles on the 'flat slope' topography with a 2 m slope and a 1 m slope, respectively. The model predicts a slight increase of deposit densities downstream of the slope break both in runs B1 and B5. The peaks are distinctive in runs using sieved particles (B3 and B7), but disappear in several other runs. The total amounts of deposit decreases and the peaks are less distinctive in runs using a dilute suspension (B2 and B6) and in runs using a shorter lock-gate (B4 and B8).

These profiles are plotted together with the results of experiments in Figs. 3.15 - 3.18. The model predictions in Fig. 3.15 show good agreement with experiments for the positions of the maxima in the deposit density profiles, but the peaks are lower than those in the experiments. The peaks in Figs 3.16 and 3.18 are less distinctive partly due to the small amounts of total deposit.

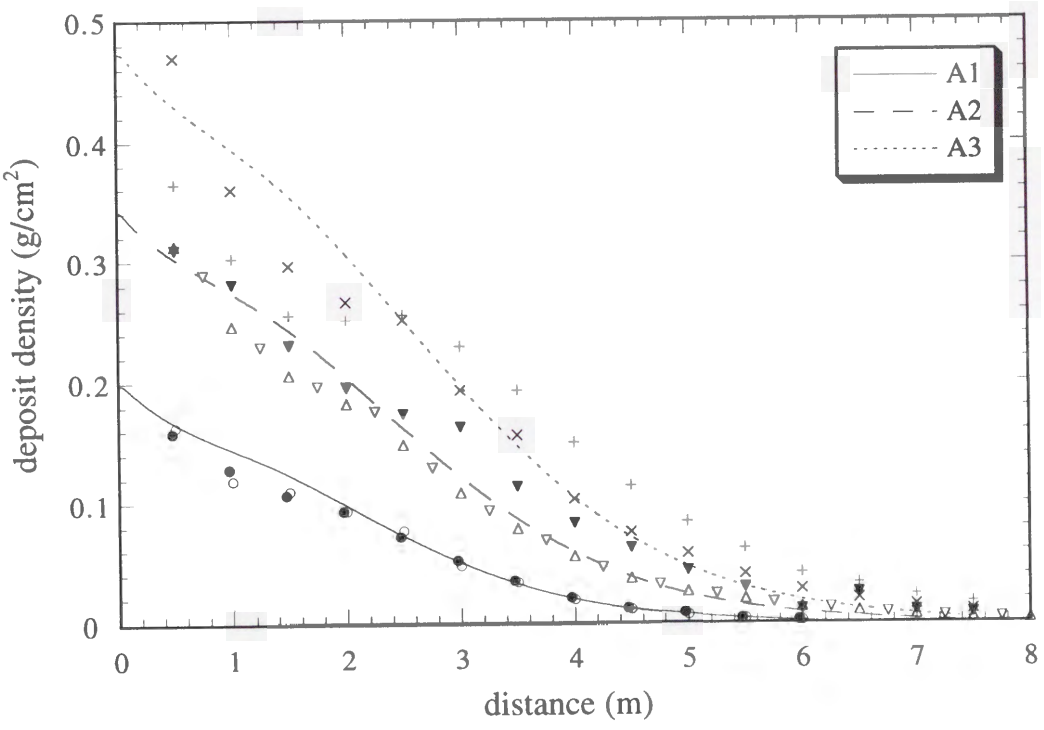

Fig. 3.12. Model predictions of the deposit density profile on the flat bed for various sediment concentrations, plotted together with the results of experiments shown in Fig. 3.5.

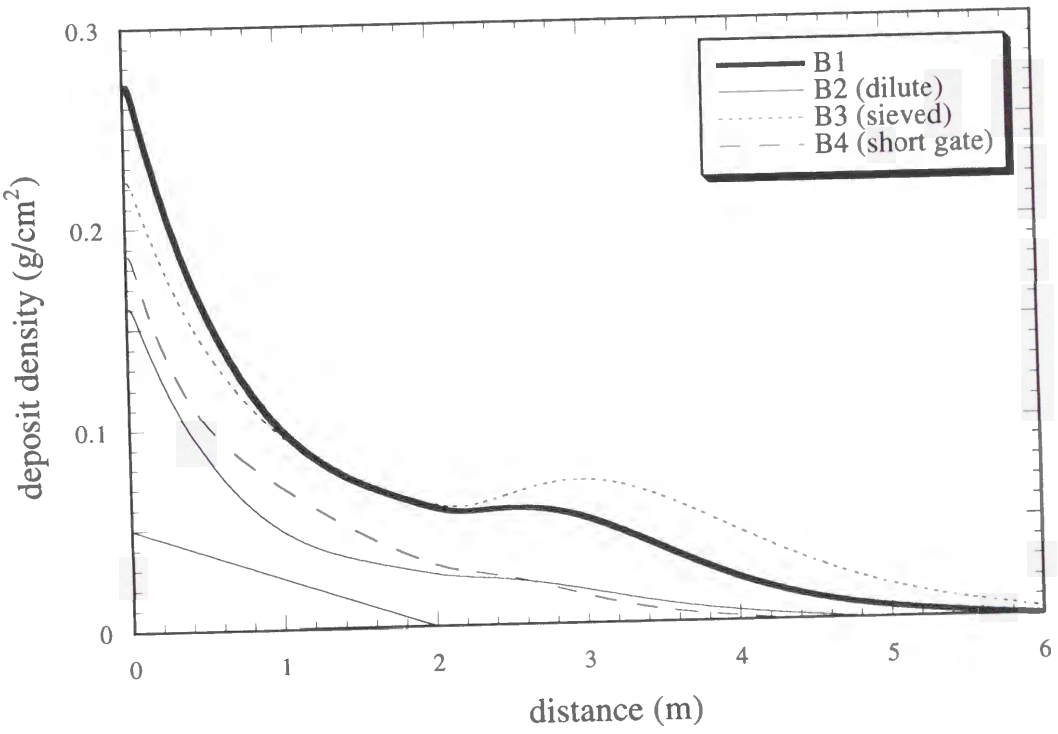

Fig. 3.13. Model predictions of the deposit density profiles for various flow conditions (B1 - B4) on the flat slope topography having a 2 m slope.

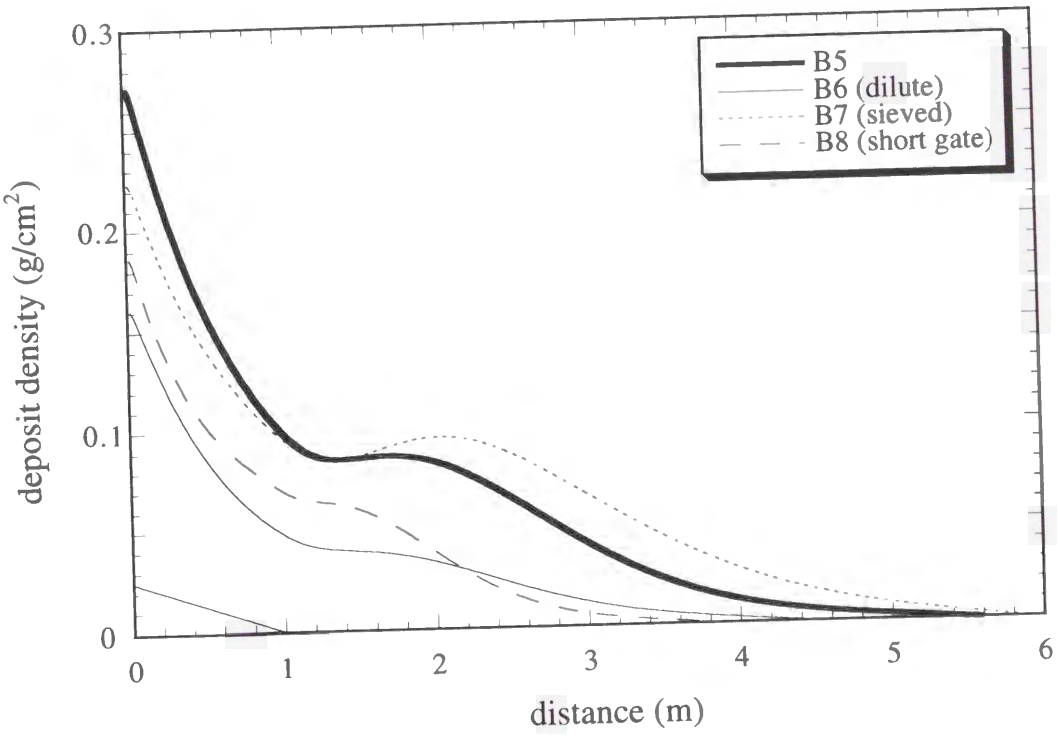

Fig. 3.14. Model predictions of the deposit density profiles for various flow conditions (B5 - B8) on the flat slope topography having a 1 m slope.

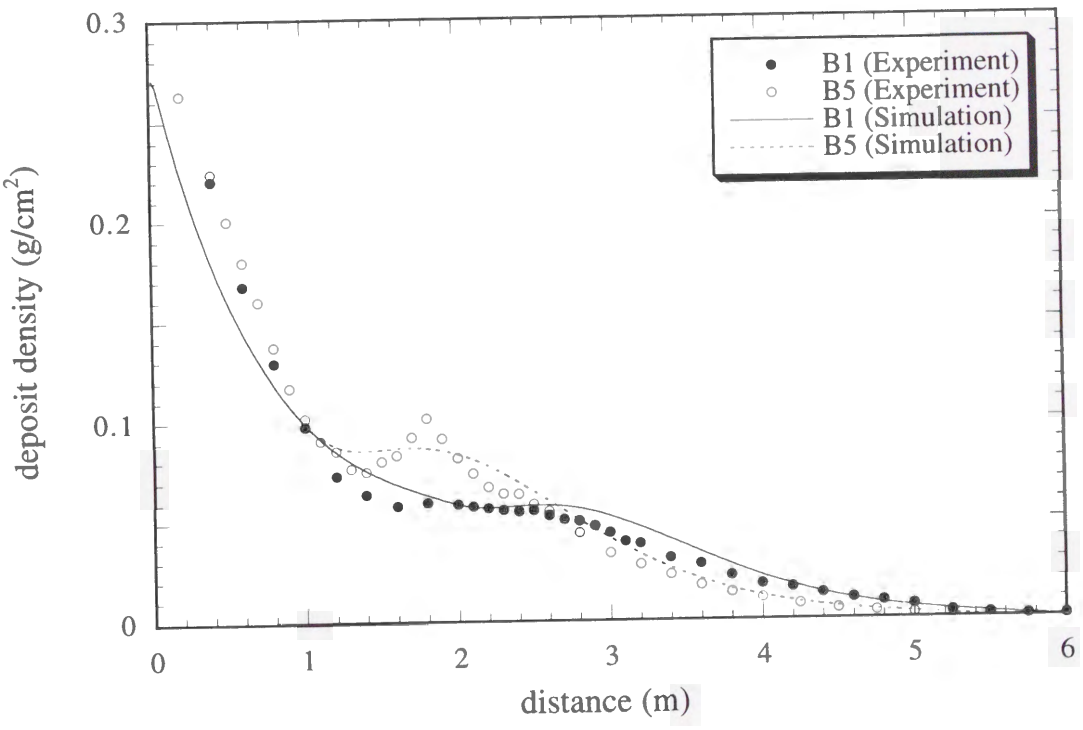

Fig. 3.15. Model predictions of the deposit density profiles on the flat slope topography, plotted together with the results of experiments (B1 and B5).

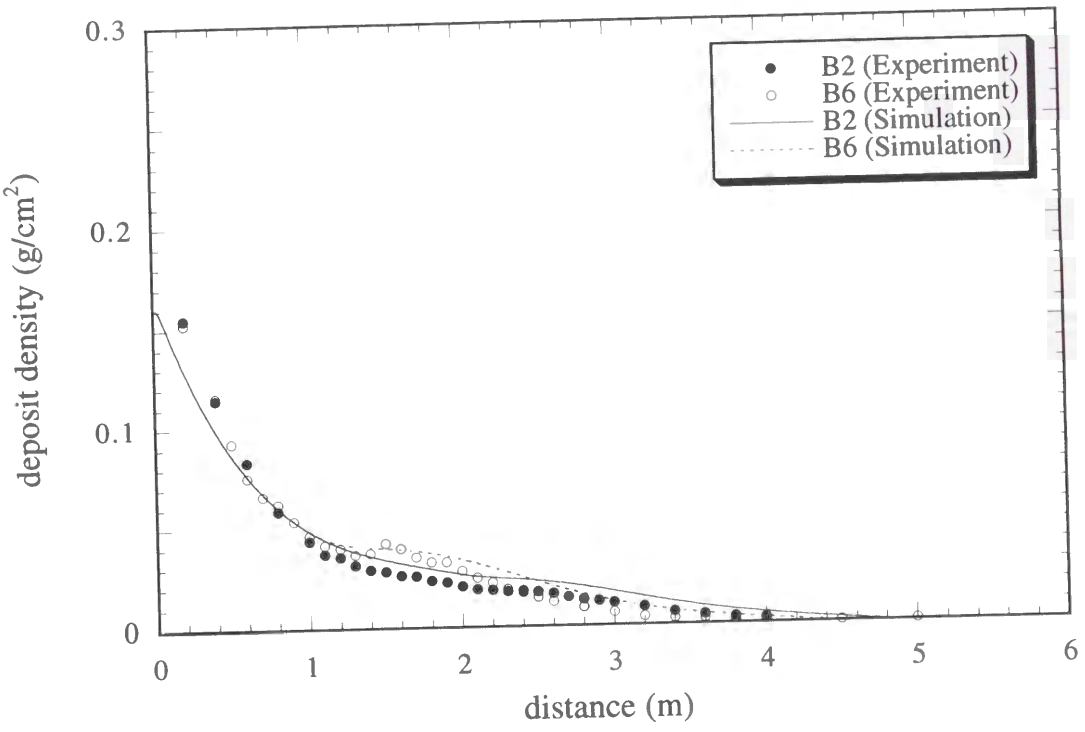

Fig. 3.16. Model predictions of the deposit density profiles on the flat slope topography, plotted together with the results of experiments (B2 and B6). The flows are dilute compared with those in Fig. 3.15.

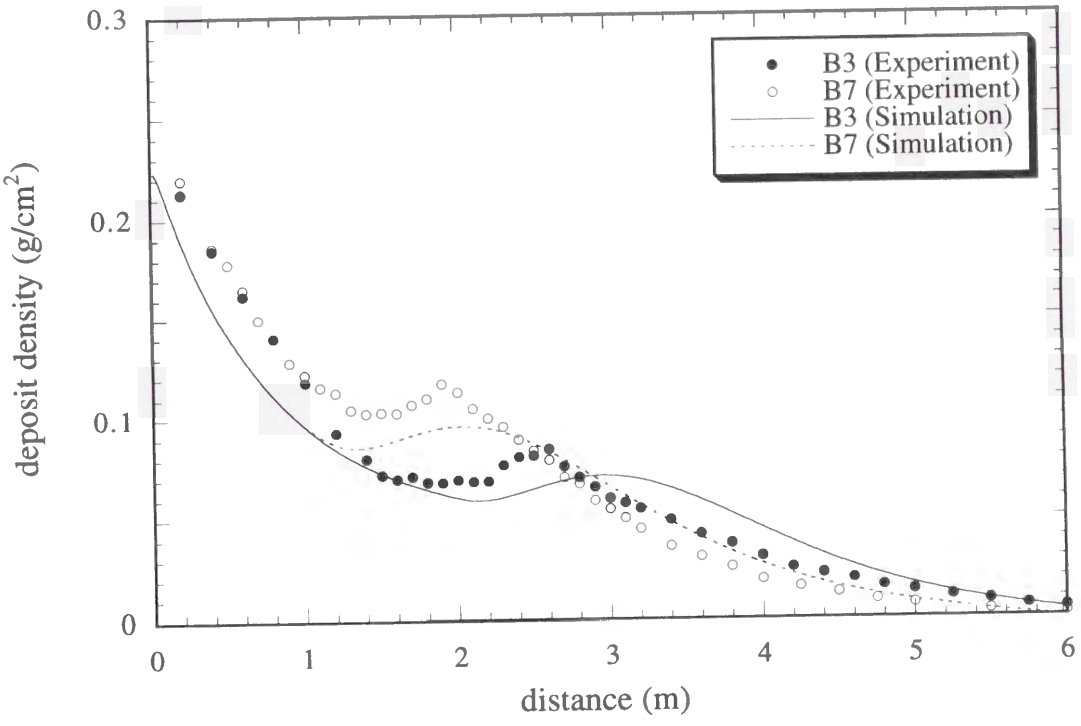

Fig. 3.17. Model predictions of the deposit density profiles on the flat slope topography, plotted together with the results of experiments (B3 and B7). Finer particles are used than for the flows in Fig. 3.15.

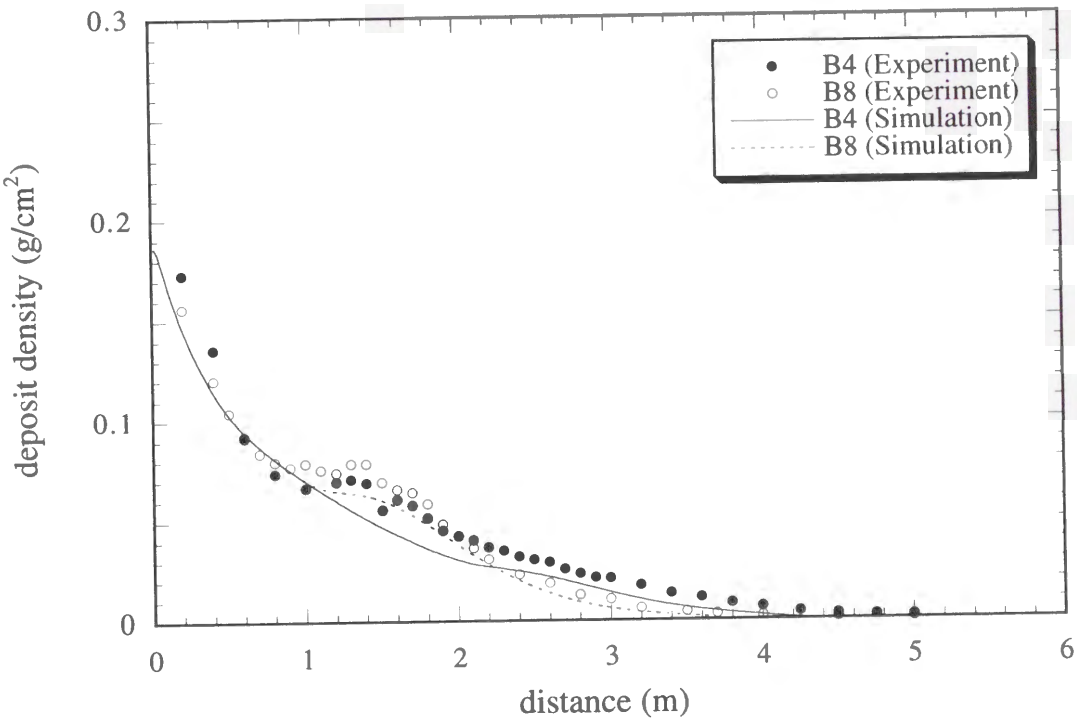

Fig. 3.18. Model predictions of the deposit density profiles on the flat slope topography, plotted together with the results of experiments (B4 and B8). A shorter gate box is used than for the flows in Fig. 3.15.

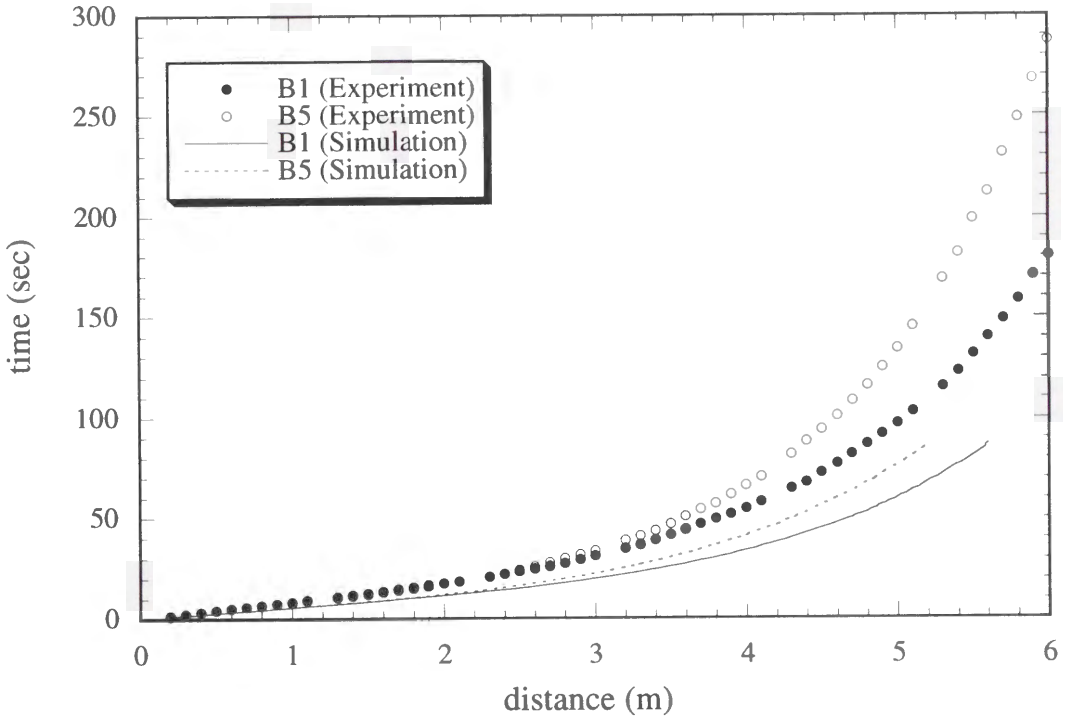

Fig. 3.19. Model predictions of the travel distance of the flow, plotted together with the results of experiments.

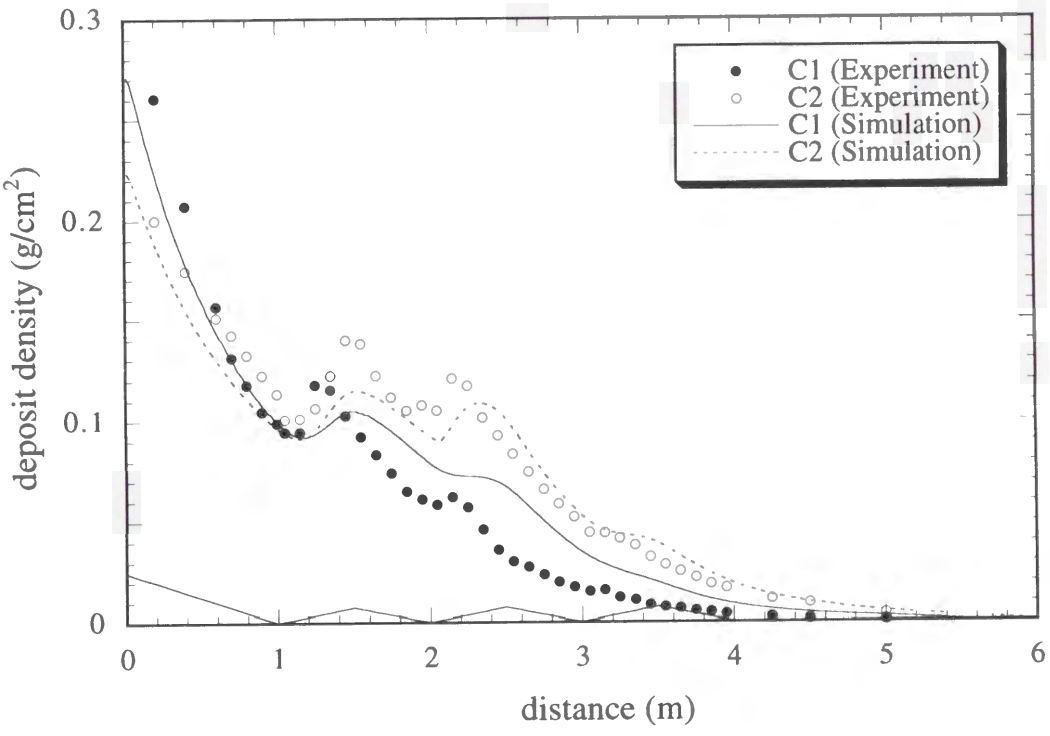

Fig. 3.20. Model predictions of the deposit density profiles on the zigzag topography, plotted with the results of experiments.

However, it is clear that preferential deposition takes place due to the slope break. The acute peaks in Fig. 3.17 agree with the experimental results, but the positions of the peaks are shifted downstream in the model predictions.

Figure 3.19 shows the travel distance of the head from the gate as a function of time. The model predicts earlier deceleration in B5 than in B1 due to the shorter slope. Both in B1 and B5, the flows travel faster in model predictions than in experiments.

Third series: On the 'zig-zag' topography, the model predicts peaks on every upslope in the deposit density profile (Fig. 3.20). The profiles agree with experimental results in general, but the peaks are lower than and located downstream of the peaks in the experiments.

Application to natural settings

The model predictions of the thickness variation of a turbidite bed on a constant slope are plotted in Figs. 3.21 - 3.28 for various combinations of initial conditions. The thickness variations show either monotonous decrease or peaks after a proximal decrease. It should be noted that the peaks are, especially when the smaller settling velocity is used, found even on constant slopes. Although the controlling factor for the appearance of the peaks can not be determined, it seems that flows diminish before reaching the points of peaks when the larger settling velocity is used. All profiles show that the flows are depositional, i.e., net deposition occurs even though local erosion possibly takes place.

Some of the most likely cases are selected from Figs. 3.21 - 3.26 for the simulation of sediment wave formation. The cases in Fig. 3.27 and Fig. 3.28 are precluded because the beds are inconsistent with general observations of natural deposits on submarine levees regarding thickness (Fig. 3.27) and lateral extent (Fig. 3.28).

The model predicts the development of the wavy structures by repeated deposition of turbidites on an initially flat bed (Fig. 3.29). The initial conditions employed are the same as those for #1 in

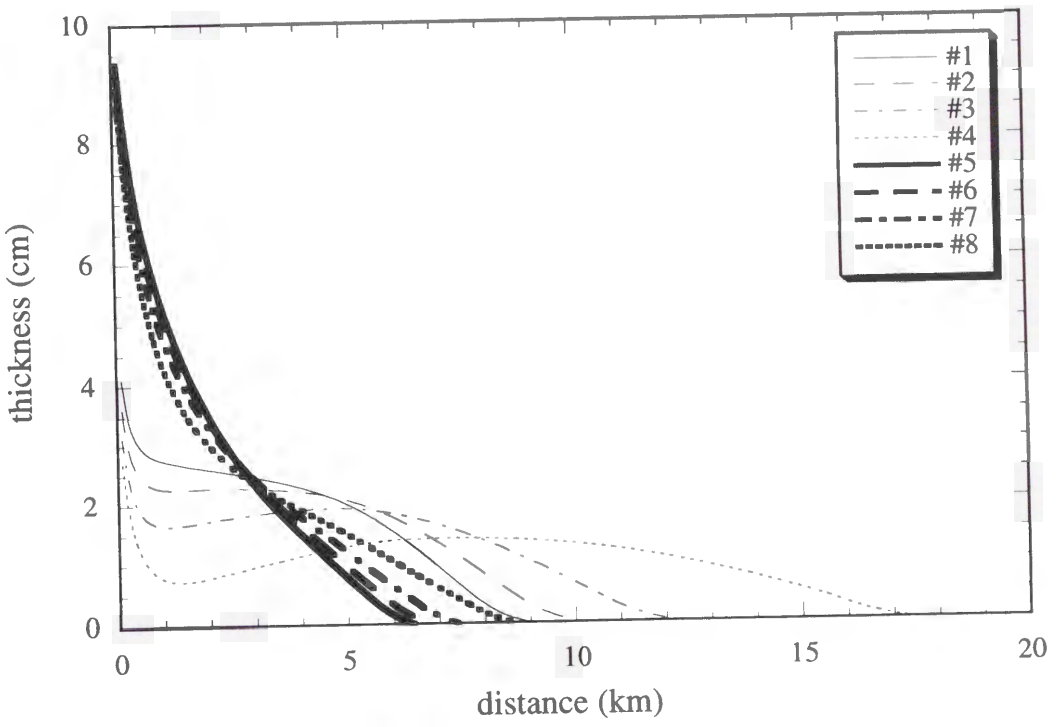

Fig. 3.21. Model predictions of the thickness profiles of single turbidite beds (initial particle concentration C =0.001, initial suspension height H =50 m, supply duration of suspension T =60 min). The settling velocity of particles is 0.3 cm/s in #1 - #4 and 1.0 cm/s in #5 - #8. The initial slope is 0 (flat) in #1 and #5, 0.002 in #2 and #6, 0.005 in #3 and #7, and 0.01 in #4 and #8.

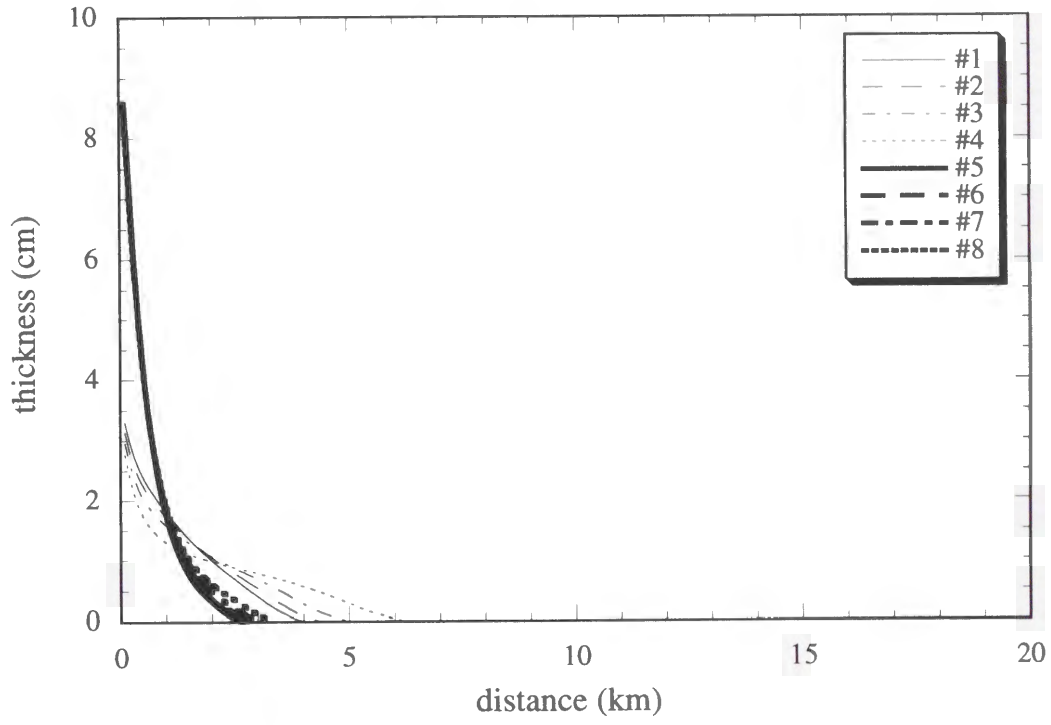

Fig. 3.22. Model predictions of the thickness profiles of single turbidite beds (C =0.001, H =20 m, T =60 min). See Fig. 3.21 for plot marks.

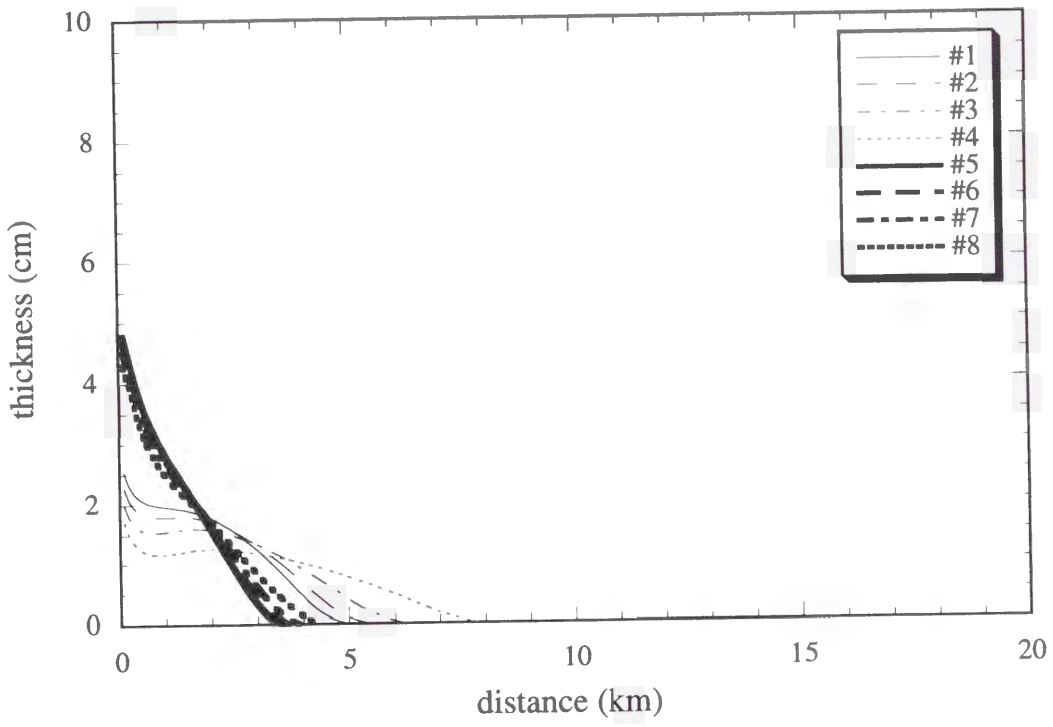

Fig. 3.23. Model predictions of the thickness profiles of single turbidite beds (C =0.001, H =50 m, T =20 min). See Fig. 3.21 for plot marks.

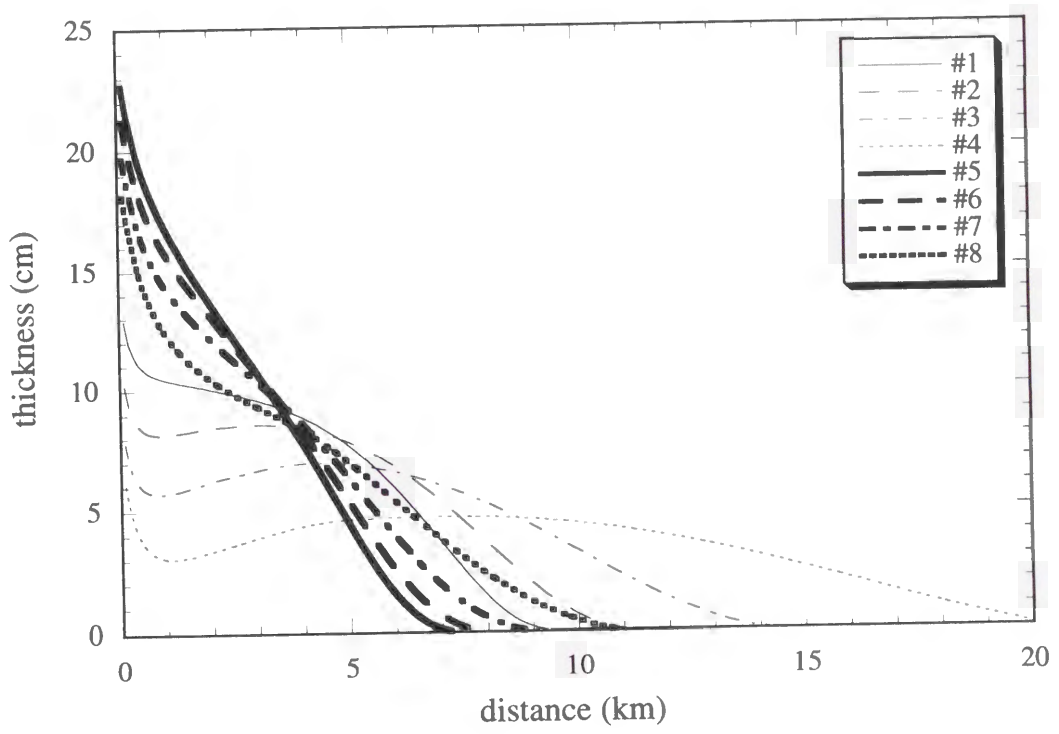

Fig. 3.24. Model predictions of the thickness profiles of single turbidite beds (C =0.005, H =50 m, T =20 min). See Fig. 3.21 for plot marks.

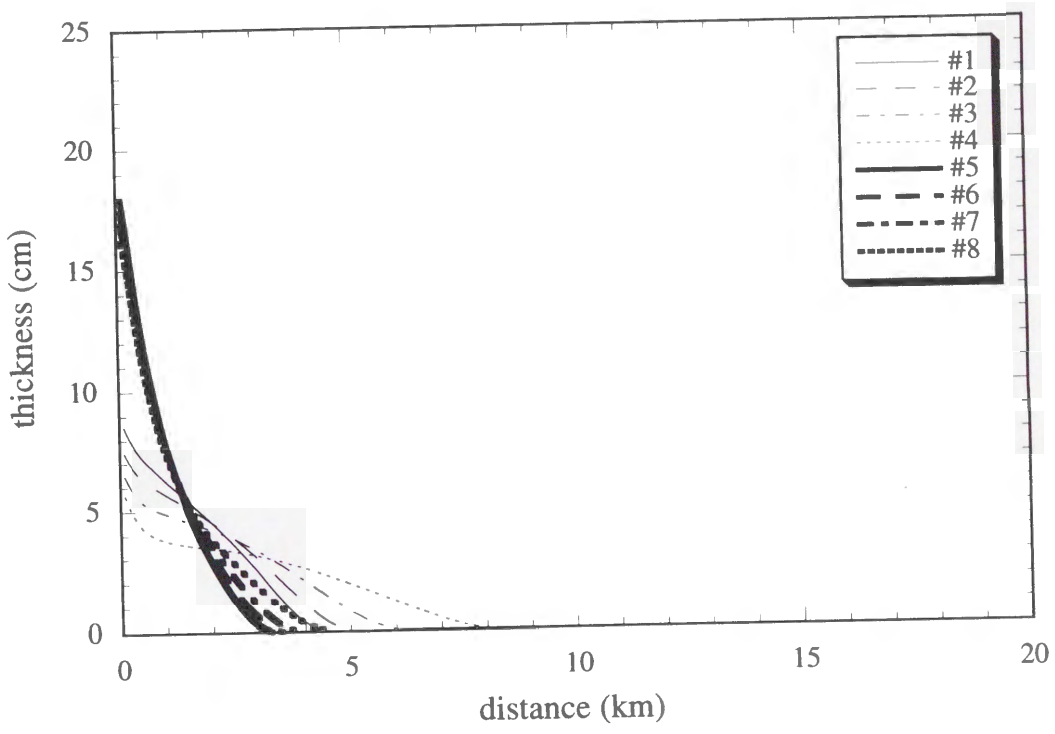

Fig. 3.25. Model predictions of the thickness profiles of single turbidite beds (C =0.005, H =20 m, T =20 min). See Fig. 3.21 for plot marks.

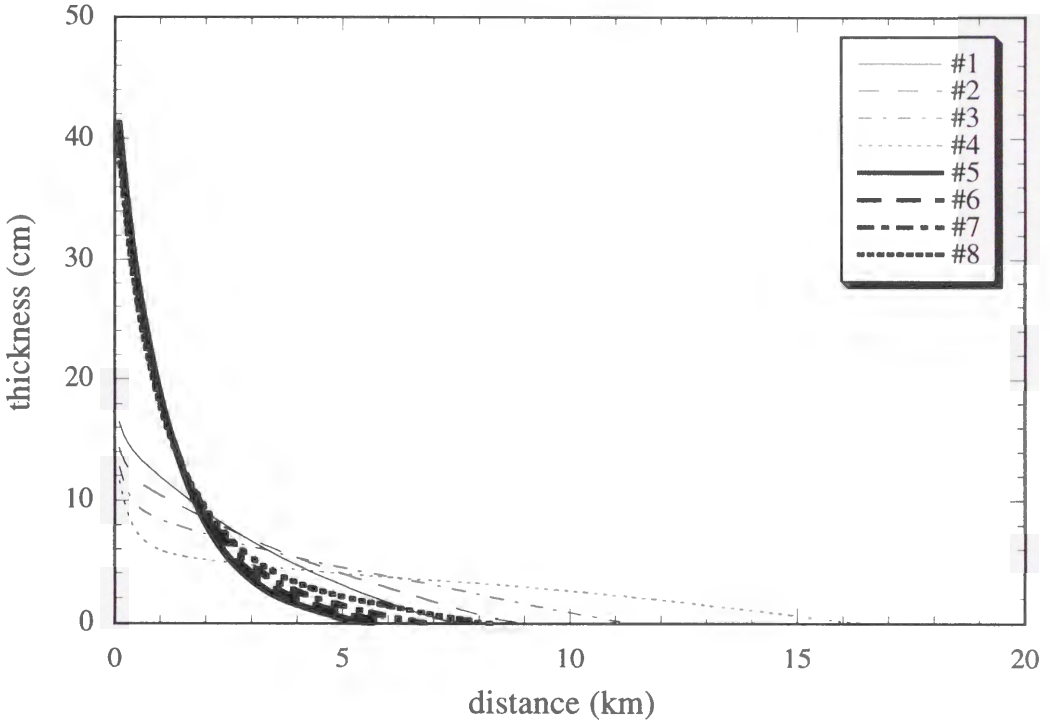

Fig. 3.26. Model predictions of the thickness profiles of single turbidite beds (C =0.005, H =20 m, T =60 min). See Fig. 3.21 for plot marks.

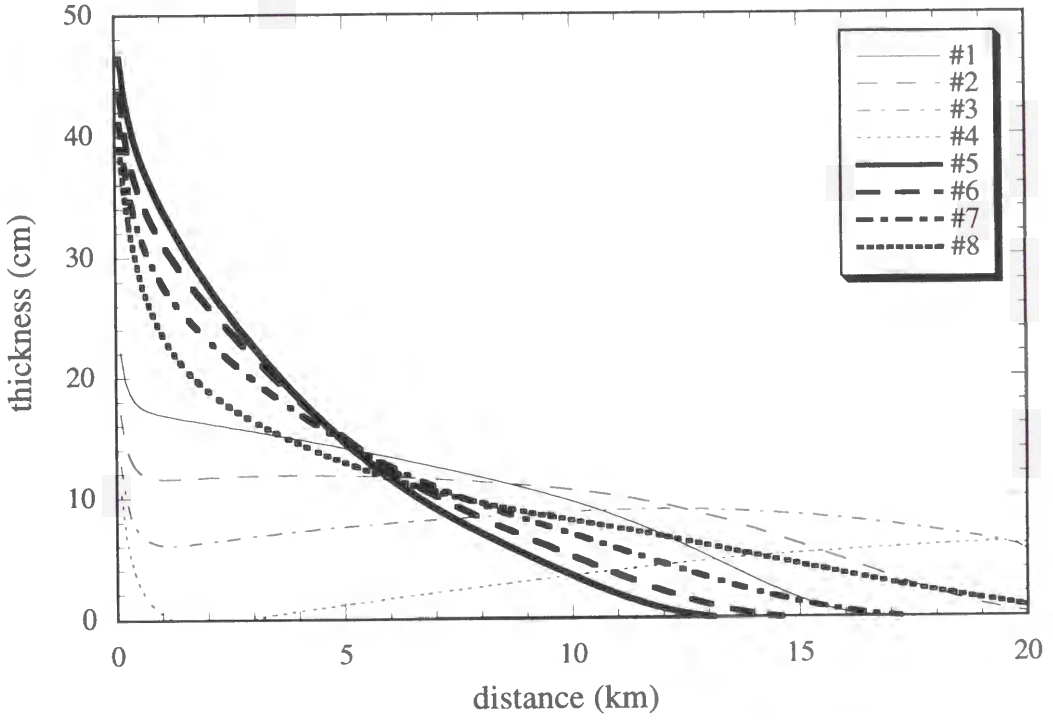

Fig. 3.27. Model predictions of the thickness profiles of single turbidite beds (C =0.005, H =50 m, T =60 min). See Fig. 3.21 for plot marks.

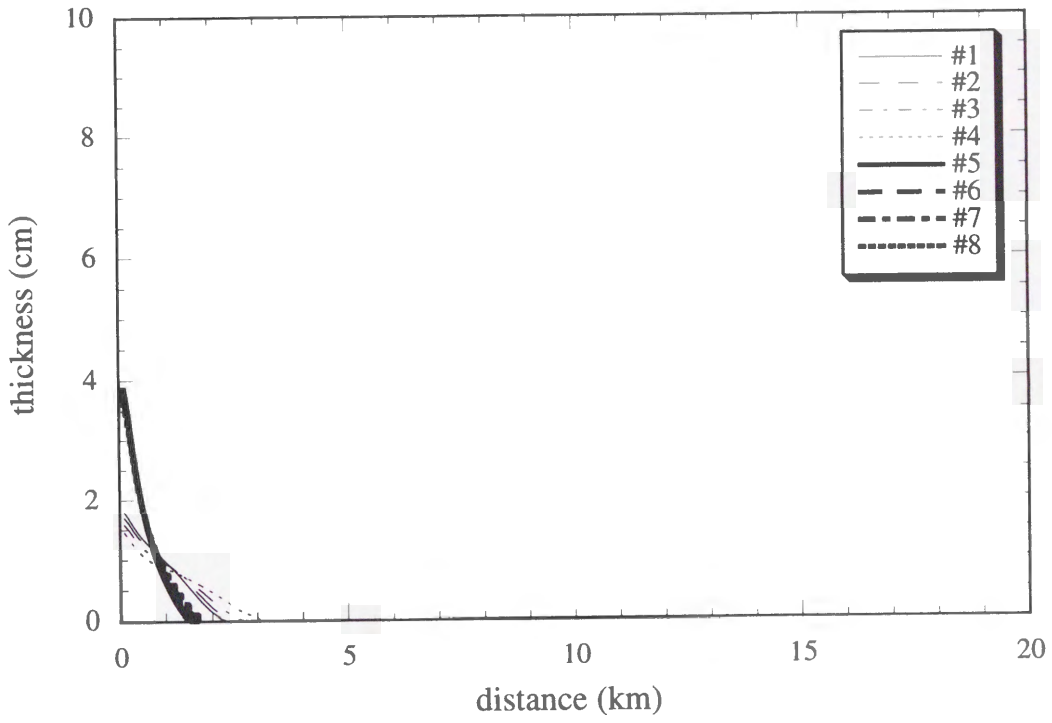

Fig. 3.28. Model predictions of the thickness profiles of single turbidite beds (C =0.001, H =20 m, T =20 min). See Fig. 3.21 for plot marks.

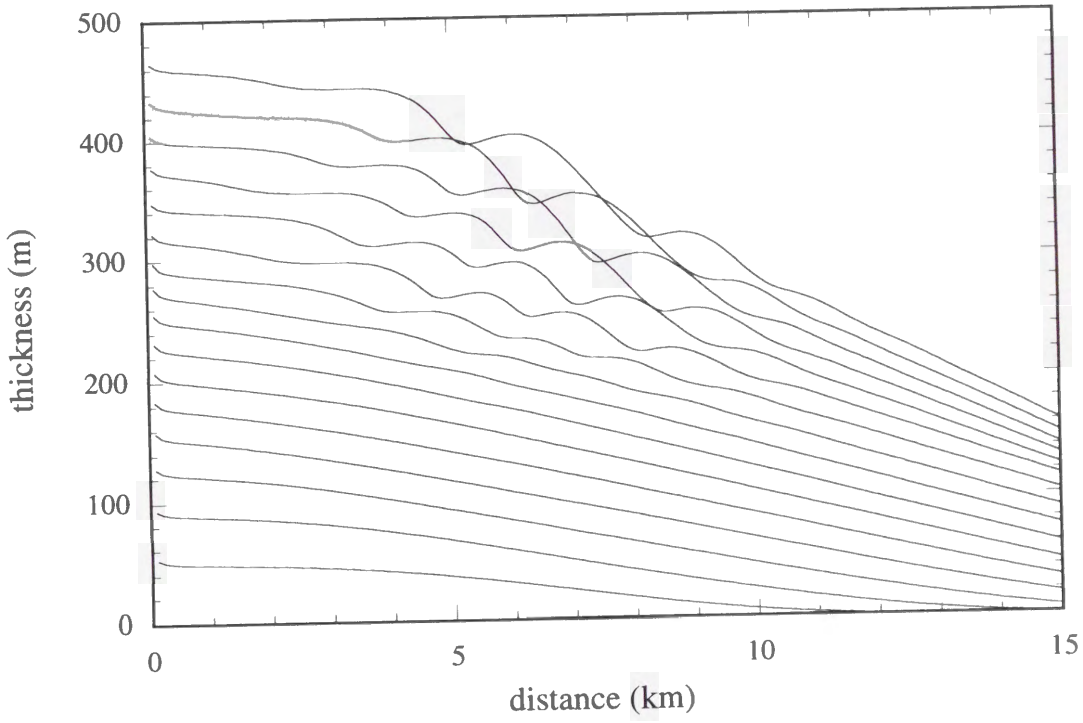

Fig. 3.29. The model prediction of the development of the wavy structures by repeated deposition of turbidites on an initially flat bed. The initial conditions are the same as those for #1 in Fig. 3.24. Each layer represents 50 time intervals of calculation, corresponding to 500 turbidite beds. The waves have an apparent wavelength of 1 - 2.5 km and maximum height of 80 m. Note the upstream migration of the waveform.

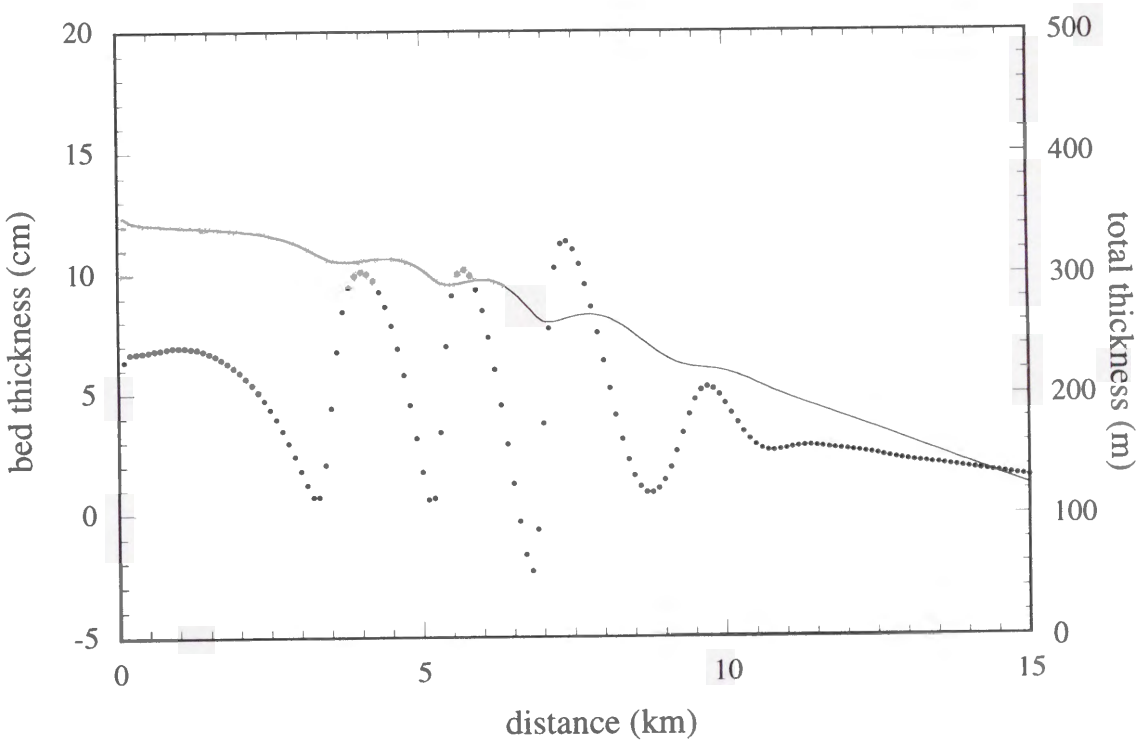

Fig. 3.30. The relationship between the topography and thickness variation of a single turbidite bed at the 600th deposition in the wavy structure shown in Fig. 3.29. The normal line is the topography at the 600th depositionand the bold points show the thickness variation of the 600th turbidite bed. Note the preferential deposition on upstream flanks of the wavy topography.

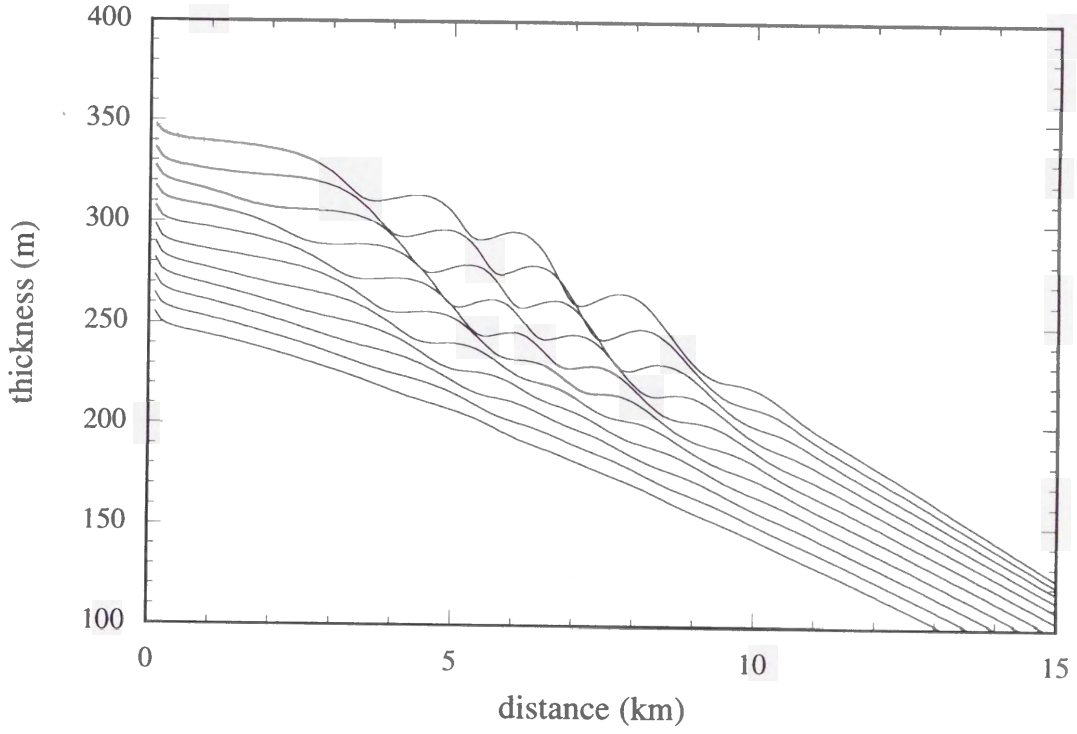

Fig. 3.31. Enlarged wavy structure in Fig. 3.29 (400 - 600th beds). Each layer represents 20 time intervals of calculation, corresponding to 200 turbidite beds. The development of the wavy structure is initiated by preferential deposition after a slope change at about 5 km from the source. The first mound develops 0.5 - 1.0 km downstream from the slope break.

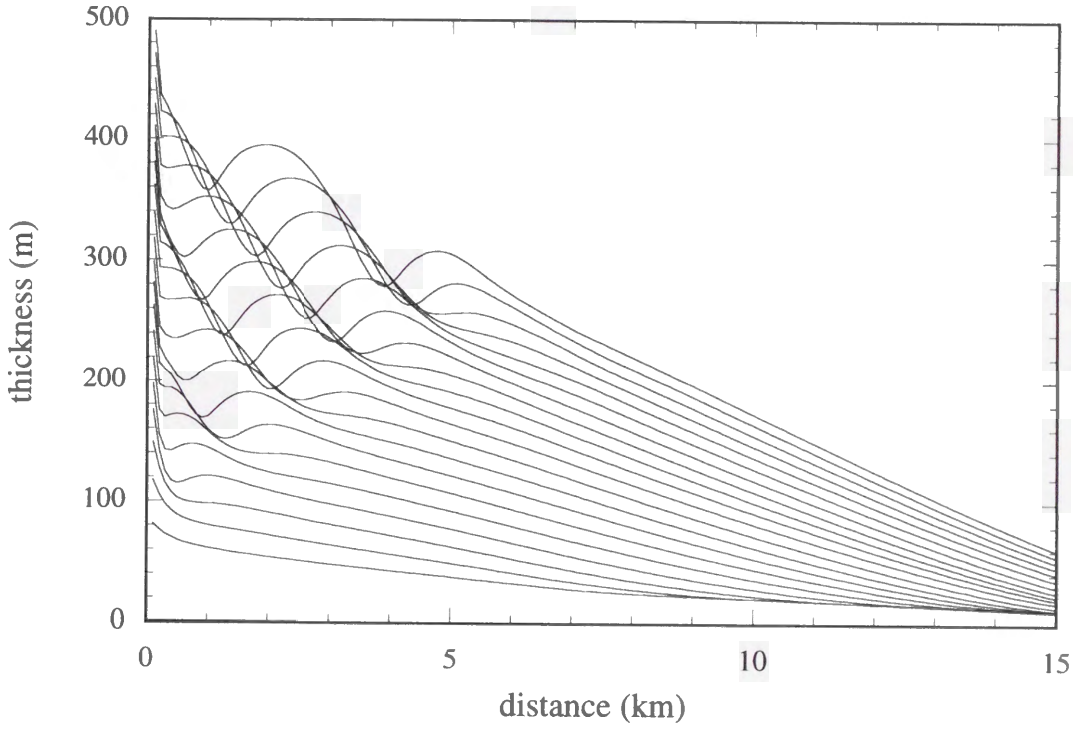

Fig. 3.32. The model prediction of the development of the wavy structures by repeated deposition of turbidites on an initially constant slope. The initial conditions are the same as those for #6 in Fig. 3.21. Each layer represents 50 time intervals of calculation, corresponding to 500 turbidite beds. The waves have an apparent wavelength of 1 km and maximum height of 100 m. The wave formation is initiated by the first slope break at 0.3 - 0.4 km from the source. The first mound develops 0.6 - 0.7 km downstream from the slope break, and the process is repeated until the development of the fifth mound after deposition of 10000 turbidites.

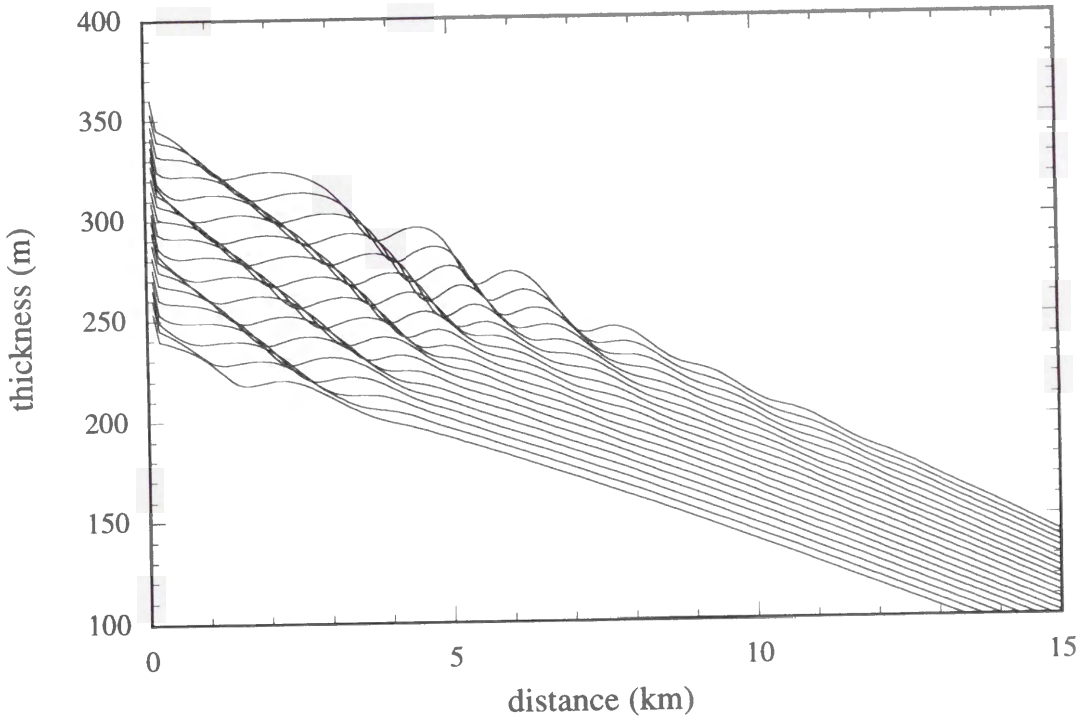

Fig. 3.33. The model prediction of the development of the wavy structures from the 360th to the 550th deposition of turbidites on an initially flat bed. The initial conditions are the same as those for #1 in Fig. 3.26. Each layer represents 10 time intervals of calculation, corresponding to 100 turbidite beds. Note the crossing of layers indicating net erosion on the downstream flanks of the waves.

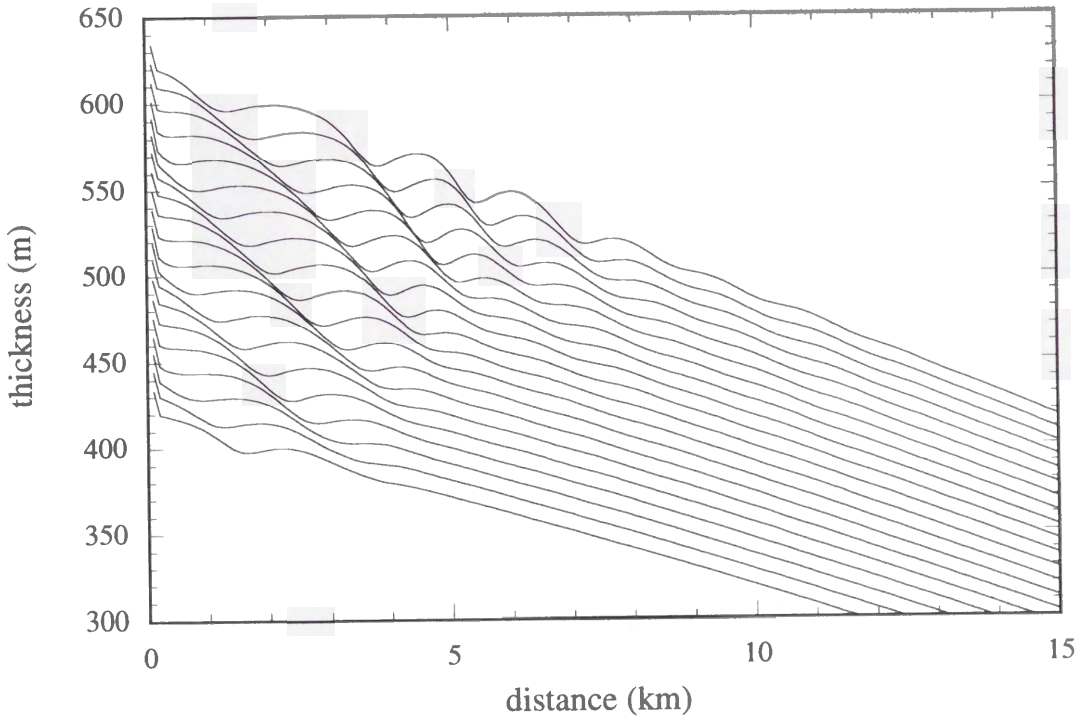

Fig. 3.34. The wavy structure in Fig. 3.33 with modification by 5 cm thick pelagic sedimentation after each turbidite interval. There is no crossing of layers that would indicate net erosion.

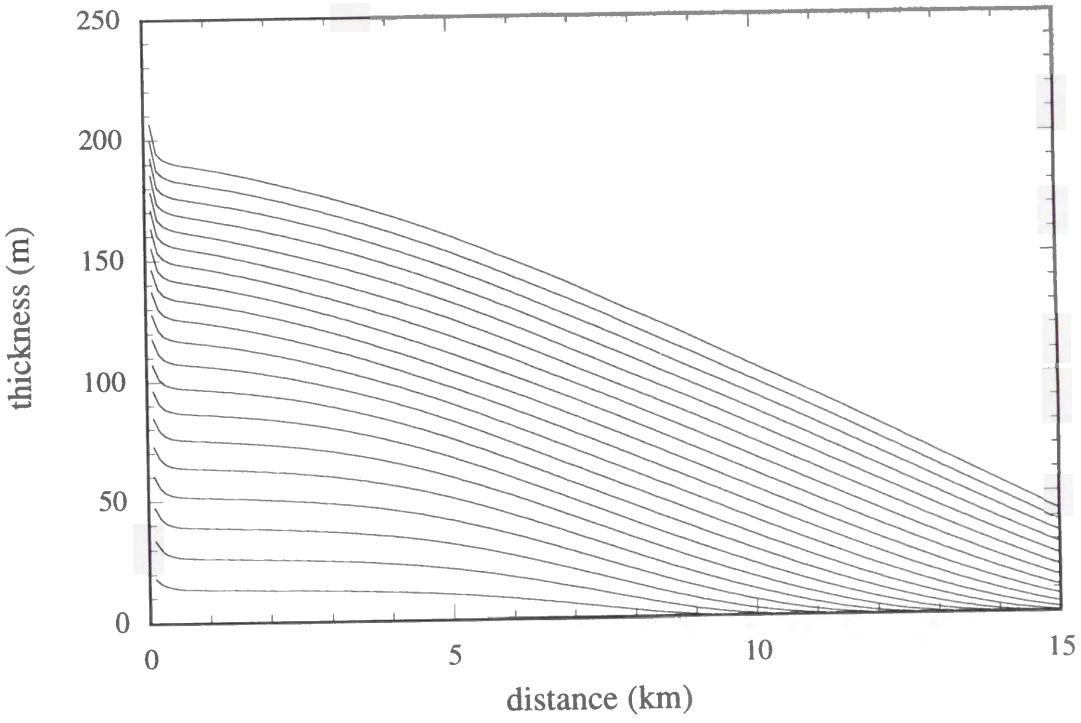

Fig. 3.35. An example of monotonous accumulation of turbidites. The initial conditions are the same as those for #1 in Fig. 3.21. No undulation is developed by 1000 times repetition of calculations (=10000 turbidites).

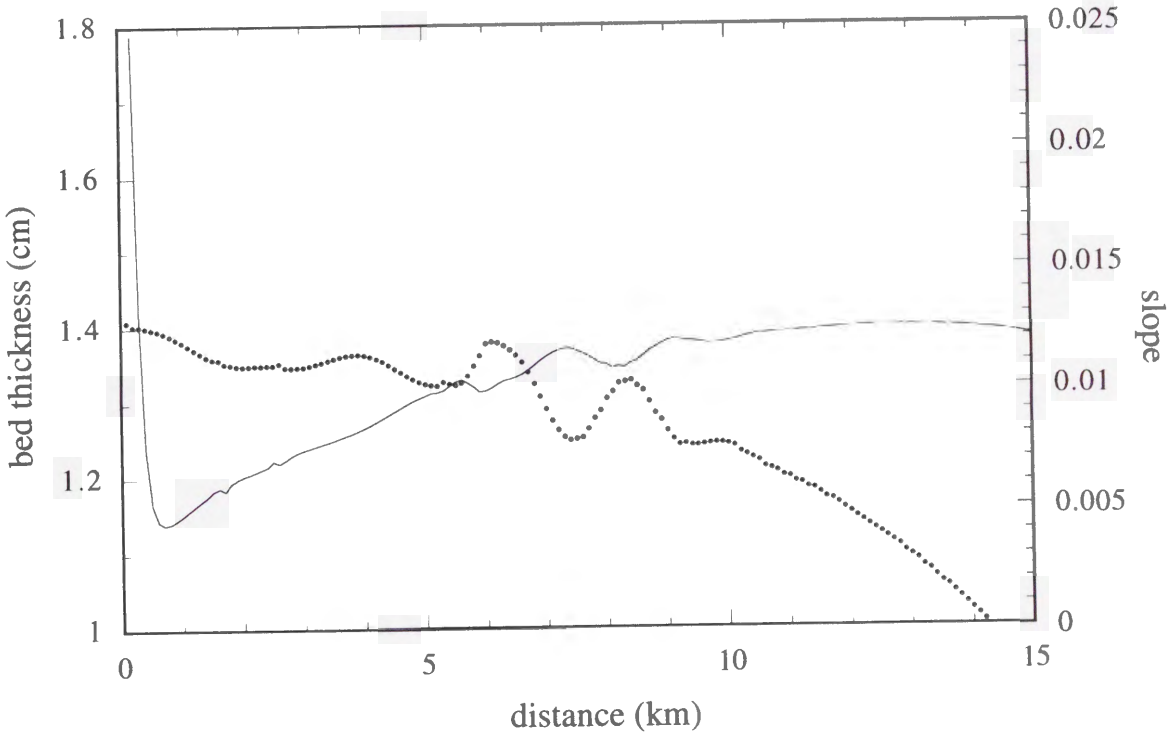

Fig. 3.36. Thickness (bold points) and slope variation (normal line) of a single turbidite bed at the 1000th deposition in Fig. 3.35.

Fig. 3.24. Each layer represents 100 time intervals of calculation, corresponding to 1000 turbidite beds. The waves have the apparent wavelength of 1 - 1.5 km and maximum height of 40 - 50 m. The internal layering displays upstream migration of the waveform due to differential deposition. Figure 3.30 shows the relationship between the topography and thickness variation of single turbidite bed. It is clear that preferential deposition takes place on upstream flanks of the wavy topography.

It should be noted that each mound in the wavy structure develops individually, rather than as consecutive waves forming simultaneously. Each mound is formed by preferential deposition somewhat downstream of a change of slope. In Fig. 3.29, the development of the wavy structure is initiated by preferential deposition after a slope change at about 5 km from the source. The first mound develops 0.5 - 1.0 km downstream from the slope break (Fig. 3.31). As the mound grows, a new slope break is formed on the downslope side of the mound and produces the second mound at 6.5 km from the source. In Fig. 3.29, this process is repeated until the development of the fifth mound.

This process can be seen better in Fig. 3.32, in which the flow conditions are the same as those of #6 in Fig. 3.21. The waves have an apparent wavelength of 1 km and maximum height of 100 m. The wave formation is initiated by the first slope break at 0.3 - 0.4 km from the source (Fig. 3.32), which is formed by accumulation of concave-up profiles of turbidite beds on a constant slope (Fig. 3.21 #6). The first mound develops 0.6 - 0.7 km downstream from the slope break, and the process is repeated until the development of the fifth mound after deposition of 10000 turbidites.

The crossing of layers in Fig. 3.29 and Fig. 3.32 means net erosion on the downstream flanks of the waves, where the slope exceeds 1/10 locally. Erosional features are observed on gentler slopes in Fig. 3.33, in which the flow conditions are the same as those of #1 in Fig. 3.26. These erosional features are, however, possibly canceled by pelagic sedimentation intercalated in turbidite beds. Figure 3.34 shows a case where the crossing of layers shown in Fig. 3.33 is lost by adding 5

cm thick pelagic sedimentation after each turbidite interval.

The wavy structure is not necessarily developed in all cases. An example of monotonous accumulation of turbidite is shown in Fig. 3.35, in which the flow conditions are the same as those of #1 in Fig. 3.21. No undulation can be observed in the topography developed by 1000 times repetition of calculations (=10000 turbidites), even though each bed shows undulation in thickness reflecting a slight variation in slope after the deposition of all the beds (Fig. 3.36).

3.3.4 Discussion

The numerical model gives, in general, successful results in simulating the deposition from turbidity currents in laboratory experiments. However, the model predicts less acute peaks in the deposit density profiles in several cases. As discussed in the previous section, the acute peaks in the deposit density profiles in laboratory experiments are possibly attributed to turbulence generated by hydraulic jump at the slope break. Effects of a discontinuous phenomenon such as a hydraulic jump is can not be evaluated in the numerical model based on layer-averaged equations.

In all runs, the model predicts less deposits in the upstream area and more in the downstream area, i.e. particles are deposited earlier in experiments than predicted by the model. The early deposition is considered to result from a vertical gradient in particle concentration within the flow. Whereas a uniform suspension is assumed in the model, particles are actually concentrated in the lower part of the flow. Even at the beginning of the experiment, the concentration gradient is possibly formed as a result of the 2 sec interval before removing the lock-gate. Although the sediment loss in the interval is taken into consideration in the model, the concentration gradient is not incorporated in layer-averaged equations. The sediment loss in upstream areas results in earlier deceleration of the flow than the model predicts.

The early deposition is also observed in the third series on the "zig-zag" topography, on which the "ponding" of the sediments takes place. The ponding occurs when the sediments in the lower

part of the flow are unable to get over the topographic high. The ponding in experiments should be more effective than in model predictions due to the vertical gradient of sediment concentration within the flow.

On the zigzag topography, there is a disagreement on the positions of peaks in deposit density profiles between the model prediction and the results of experiments. The model predicts that the peaks in the deposit density profiles are located near the crests of the zigzag topography, whereas some peaks in the experiments are at the middle of the upslope. While a hydraulic jump is a possible cause for these gaps, it is likely that partial blocking of the flow and more ponding of the sediments results in preferential deposition at the middle of upslopes.

In the simulation of large scale turbidity currents on submarine levees, the model predicts that wavy structure is developed by repeated accumulation of turbidite beds. The waves show features similar to natural sediment waves for the length scale and the pattern of internal layering. The predictions of the model, even though oversimplified to evaluate the wave features quantitatively, present qualitative speculations on the process of sediment wave formation by turbidity currents.

The wavy structure is developed as a train of mounds which are formed individually by preferential deposition near changes of slope. Therefore, the conditions for the wave formation can not be defined directly by the flow conditions nor by specific fluid motion such as lee waves and supercritical flows. Rather, the slope variation and the resultant wave formation are almost inevitable in accumulation of turbidite beds, considering that the thickness of each turbidite can not be uniform throughout the depositional area.

In the model predictions, no more than 4 - 5 crests are formed during the deposition of five to ten thousands turbidite beds, whereas more than 10 crests are observed in some sediment wave fields (e.g. Carter *et al.*, 1990; Nakajima, 1996). It is unlikely that the sediment wave field consists of more than tens of thousands of turbidite beds, considering the frequency of turbidity current occurrence and the time-scale of eustatic sea-level changes. Nakajima (1996) estimated intervals of flow-stripping turbidity currents in the Toyama Deep Sea channel as more than 300 years. It should

take, therefore, at least several million years for the wave development by 10,000 turbidite beds. On the other hand, Carter *et al.* (1980) interpreted that development of the sediment wave field on Bounty Channel levee was initiated approximately 3Ma ago and terminated before the present interglacial sedimentation. The development of the wavy structure in the numerical model is, therefore, relatively slow considering these interpretations. In addition, the wave amplitudes decrease downstream more rapidly compared to consecutive waveforms of natural sediment waves.

In nature, it is possible that these waves are formed more easily than in the numerical model. While the numerical calculations are initiated from a constant slope, it is likely that the wave formation is triggered by natural undulation of basement topography. Irregular waveforms observed in natural sediment waves on submarine levees are likely to be associated with the influence of the basement topography.

The topographic effects are more distinctive in experimental results than in numerical model predictions, probably due to turbulence within a hydraulic jump. A hydraulic jump can take place in natural turbidity currents as well. Komar (1971) stated that a hydraulic jump should occur near the change in slope in the vicinity of a canyon mouth, and estimated the slope value at critical conditions (Fr =1) as 0.0075. Hand (1974) estimated the critical slope as 0.001 from the same equation used by Komar (1971) but with a different value for the friction factor. While the estimation of the critical slope remains controversial (Komar, 1975; Hand, 1975), supercritical turbidity currents seem common in sediment wave fields on the backslopes of the levees where the slope is typically 0.005 - 0.015 (e.g. Carter *et al.*, 1980; Normark *et al.*, 1980; Nakajima, 1996). It is possible that hydraulic jumps occur at changes in slope and promote the preferential deposition resulting in sediment wave formation. The positive effects of hydraulic jumps on the preferential deposition, though the extent is unknown, could result in quick formation of the wavy structures.

The effect of hydraulic jumps on formation of wavy structure is already inferred in the experimental work of Hand (1974). Hand showed that a supercritical density current developed wavy bedforms which could be approximately described by the modified expression of the

relationship of antidune wavelength (L) and the flow depth (d) in a two-layer system:

$$L/d = 4\pi\, Fr^2$$

where Fr is the densiometric Froude number of the density current. The bedforms were described as antidunes accompanying breaking of interfacial waves, which in some cases became a submerged hydraulic jump in chutes-and-pools. The breaking of waves on antidunes, as discussed earlier in Chapter 2, can be modeled as formation and collapse of a hydraulic jump.

The antidunes produced in the experiments of Hand (1974) are similar to the wavy structure studied here. He stated that the antidunes produced by natural density currents should have wavelengths of tens to hundreds of meters, and inferred the applicability of his experimental results to deep-sea sediment waves. Several researchers have interpreted sediment waves produced by turbidity currents as antidunes of this type (Normark *et al.*, 1980; Piper and Savoye, 1993; Nakajima, 1996). The waves in the model predictions are similar to antidunes of this type as well, because of the possible, at least locally, supercritical conditions and the differential deposition on both sides of waves. The numerical model predicts wave formation by deposition from surge type turbidity currents, in which it is hard for the steady phase between the flow and the bed surface to form because of the development of the bedform. Therefore antidune-type sedimentation is not a necessary condition for sediment wave formation, though possibly takes place in a supercritical turbidity current temporarily.

Throughout the repeated calculations in the numerical model, the same initial conditions were given to generate turbidity currents. It is unrealistic to assume the same conditions as turbidity currents in nature vary in size, duration, and sediment concentration. The wide variety of flow conditions may play a negative role in formation of the wavy structure. At least, it is likely to take more time for variable flows to develop such regular morphology. However, the range of the variation should be relatively narrow in turbidity currents on levees, due to the nature of spillover from a channel. It is also possible that the variety of the flow results in irregularity of the bed, which can be a trigger for preferential deposition. It can not be judged whether the variety of the

flows works positively or negatively in the development of the wavy structure.

§4 Concluding remarks

This thesis provides new interpretations of upstream migration of bedforms including shallow water antidunes and deep water sediment waves. These interpretations are essential for a better understanding of the process of bedform migration and the resultant sedimentary structures.

The breaking of waves on antidunes is interpreted as the successive formation and collapse of a hydraulic jump. The upstream-migrating hydraulic jump transports the sediments against the flow and contributes to the establishment of a new antidune somewhat upstream of the old one. The theoretical considerations in this study establish the flow conditions for hydraulic jump, and show this process to be consistent with a cycle of events commonly observed in laboratory experiments of antidunes. The bedform migration caused by this cycle is unique to antidunes, and therefore may be regarded as a key feature in identifying antidune sedimentation.

It is still difficult to predict the detailed features in sedimentary structures formed by the hydraulic jump. An expansion of this study must include considerations on sediment movement in a turbulent flow. Lateral cyclicity and curvilinearity of antidune waveforms must be also considered, as antidunes are characterized by their symmetric and sinusoidal profile.

Sediment wave formation in the deep sea is interpreted to be caused by preferential deposition from turbidity currents after a change of slope. The results of the experiments in a laboratory flume in this study show that preferential deposition actually takes place after a slope break. It is also shown that the differential deposition occurs on both sides of the wavy topography, implying the possible upstream migration of the waveform. The numerical model simulating spillover turbidity currents on abyssal levees predicts the development of wavy structures after accumulation of thousands of turbidite beds. The wave formation is initiated by preferential deposition after a change of slope and developed by differential deposition on both sides of the wavy topography. The wave features in the model predictions are similar to those of natural sediment waves for the length of the waves and the pattern of internal layering. It is worth noting that the wave formation in

the model predictions requires no specific fluid motions, such as lee waves and phase equivalence in supercritical flow.

Unfortunately the numerical model is unable to establish any quantitative relationship between the flow conditions and the bedform features such as wavelength and migration rate. Further improvements are required in the numerical model, specifically in the parameterization of the sediment movement within a turbidity current, to obtain such relationships. The necessary or critical condition for the sediment wave formation can not be determined either. It will be possible, however, to put a restriction on the combination of the flow and the boundary conditions in the case studies of a specific sediment wave field in nature.

Acknowledgements

I am mostly grateful to Prof. Fujio Masuda, Kyoto University, for his supervision and support to this study. I am grateful to Prof. T. Sunamura and members of Geoenvironment Science Laboratory of Osaka University for their permission and cooperation in conducting flume experiments: notably Dr. M. Yokokawa kindly provided the figure in Chapter 2 and informative discussions. I am also grateful for helpful comments from M. Felix of University of Leeds, who reviewed an earlier draft of this manuscript, T. Sakai of Kyoto University and T. Nakajima of Geological Survey of Japan. This study has been supported by a Grant-in-Aid for Scientific Research from the Ministry of Education of Japan and a research fellowship of the Japan Society for the Promotion of Science for Young Scientists.

References

Akiyama, J. and Stefan, H.G., 1988, Turbidity current simulation in a diverging channel. *Water Resour. Res.*, **24**, 579-587.

Alexander, J. and Morris, S., 1994, Observations on experimental, nonchannelized, high-concentration turbidity currents and variations in deposits around obstacles. *J. Sedim. Res.*, **A64**, 899-909.

Allen, J.R.L., 1966, On bed forms and paleocurrents. *Sedimentology*, **6**, 153-190.

Allen, J.R.L., 1982a, *Sedimentary structures: their character and physical basis*, Vol. I. Elsevier, Amsterdam, 593pp.

Allen, J.R.L., 1982b, *Sedimentary structures: their character and physical basis*, Vol. II. Elsevier, Amsterdam, 663pp.

Allen, J.R.L., 1991, The Bouma division A and the possible duration of turbidity currents. *J. Sedim. Petrol.*, **61**, 291-295.

Asquith, S.M., 1979, Nature and origin of the lower continental rise hills off the east coast of the United States. *Mar. Geol.*, **32**, 165-190.

Baines, P.G., 1988, A general method for determining upstream effects in stratified flow of finite depth over long two-dimensional obstacles. *J. Fluid Mech.*, **188**, 1-22.

Baines, P.G., 1995, *Topographic effects in stratified flows*, Cambridge University Press, Cambridge, 482pp.

Ballard, J.A., 1966, Structure of the lower continental rise hills of the western North Atlantic. *Geophysics*, **31**, 506-523.

Beghin, P., Hopfinger, E.J. and Britter, R.E., 1981, Gravitational convection from instantaneous sources on inclined boundaries. *J. Fluid Mech.*, **107**, 407-422.

Benjamin, T.B., 1968, Gravity currents and related phenomena. *J. Fluid Mech.*, **31**, 209-248.

Binnie, D.J. and Orkney, J.C., 1955, Experiments on the flow of water from a reservoir through

an open horizontal channel II. the formation of hydraulic jumps. *Proc. Roy. Soc. Lond. A*, **230**, 237-246.

Blum, P. and Okamura, Y., 1992, Pre-Holocene sediment dispersal systems and effects of structural controls and Holocene sea-level rise from acoustic facies analysis: SW Japan forearc. *Mar. Geol.*, **108**, 295-322.

Blumsack, S.L. and Weatherly, G.L., 1989, Observations of the nearby flow and a model for the growth of mudwaves. *Deep-Sea Res.*, **36**, 1327-1339.

Bonnecaze, R.T., Huppert, H.E. and Lister, J.R., 1993, Particle-driven gravity currents. *J. Fluid Mech.*, **250**, 339-369.

Bonnecaze, R.T., Hallworth, M.A., Huppert, H.E. and Lister, J.R., 1995, Axisymmetric particle-driven gravity currents. *J. Fluid Mech.*, **294**, 93-121.

Bouma, A.H., 1962, *Sedimentology of some flysch deposits.* Elsevier, Amsterdam, 168pp.

Bouma, A.H. and Treadwell, T.K., 1975, Deep-sea dune-like features. *Mar. Geol.*, **19**, M53-M59.

Bowen, A.J., Normark, W.R. and Piper, D.J.W., 1984, Modeling of turbidity currents on Navy submarine fan, California continental borderland. *Sedimentology*, **31**, 169-185.

Brew, D.S. and Mayer, L.A., 1998, Modeling of Pliocene-Pleistocene abyssal mudwaves using synthetic seismograms. *Mar. Geol.*, **149**, 3-16.

Britter, R.E. and Simpson, J.E., 1978, Experiments on the dynamics of a gravity current head. *J. Fluid Mech.*, **88**, 223-240.

Britter, R.E. and Linden, P.F., 1980, The motion of the front of a gravity current traveling down an incline. *J. Fluid Mech.*, **99**, 531-543.

Buehler, J. and Siegenthaler, C., 1986, Self-preserving solutions for turbidity currents. *Acta Mechanica*, **63**, 217-233.

Carter, L., Carter, R.M., Nelson, C.S., Fulthorpe, C.S. and Neil, H.L., 1990, Evolution of Pleistocene to Recent abyssal sediment waves on Bounty Channel Levees, New Zealand.

Mar. Geol., **95**, 97-109.

Chikita, K., 1990, Sedimentation by river-induced turbidity currents: field measurements and interpretation. *Sedimentology*, **37**, 891-905.

Chu, F.H., Pilkey, W.D. and Pilkey, O.H., 1979, An analytical study of turbidity current steady flow. *Mar. Geol.*, **33**, 205-220.

Cita, M.B., Beghi, C., Camerlenghi, A., Kastens, K.A., McCoy, F.W. Nosetto, A., Parisi, E., Scolari, F. and Tomadin, L., 1984, Turbidites and megaturbidites from the Herodotus abyssal plain (eastern Mediterranean) unrelated to seismic events. *Mar. Geol.*, **55**, 79-101.

Dade, W.B., Lister, J.R. and Huppert, H.E., 1994, Fine-sediment deposition from gravity surges on uniform slopes. *J. Sedim. Res.*, **A64**, 423-432.

Dade, W.B. and Huppert, H.E., 1995, A box model for non-entraining suspension-driven gravity surges on horizontal surfaces. *Sedimentology*, **42**, 453-471.

Damuth, J.E., 1975, Echo character of the western equatorial Atlantic floor and its relationship to the dispersal and distribution of terrigenous sediments. *Mar. Geol.*, **18**, 17-45.

Damuth, J.E., 1979, Migrating sediment waves created by turbidity currents in the northern South China Basin. *Geology*, **7**, 520-523.

Damuth, J.E. and Hayes, D.E., 1977, Echo character of the East Brazilian continental margin and its relationship to sedimentary processes. *Mar. Geol.*, **24**, 73-95.

Driscoll, N.W. and Laine, E.P., 1996, Abyssal current influence on the southwest Bermuda Rise and surrounding region. *Mar. Geol.*, **130**, 231-263.

Edwards, D.A., 1993, *Turbidity currents: dynamics, deposits and reversals.* Lecture notes in earth science 44, Springer-Verlag, Berlin, 173pp.

Egloff, J., 1972, Morphology of Ocean basin seaward of northwest Africa: Canary Islands to Monrovia, Liberia. *Am. Assoc. Petrol. Geol. Bull.*, **56**, 694-706.

Eidsvik, K.J. and Brørs, B., 1989, Self-accelerated turbidity current prediction based upon (κ–ε) turbulence. *Continent. Shelf Res.*, **9**, 617-627.

Ellison, T.H. and Turner, J.S., 1959, Turbulent entrainment in stratified flows. *J. Fluid Mech.*, **6**, 423-448.

Embley, R.W. and Langseth, M.G., 1977, Sedimentation processes on the continental rise of northeastern South America. *Mar. Geol.*, **25**, 279-297.

Ewing, M., Eittreim, S.L., Ewing, J.I. and Le Pichon, X., 1971, Sediment transport and distribution in the Argentine Basin. 3. Nepheloid layer and processes of sedimentation. In: *Physics and chemistry of the Earth.* vol. 8 (Ed. by Ahrens, L.H., Press, F., Runcorn, S.K. and Urey, H.C.). Pergamon press, Oxford, 49-77.

Flood, R.D., 1988, A lee wave model for deep-sea mudwave activity. *Deep-Sea Res.*, **35**, 973-983.

Flood, R.D. and Shor, A., 1988, Mudwaves in the Argentine Basin and their relationship to regional bottom circulation patterns. *Deep-Sea Res.*, **35**, 943-971.

Flood, R.D., Shor, A. and Manley, P.L., 1993, Morphology of abyssal mudwaves at Project MUDWAVES sites in the Argentine Basin. *Deep-Sea Res. II*, **40**, 859-888.

Fox, P.J., Heezen, B.C. and Harian, A.M., 1968, Abyssal antidunes, *Nature*, **220**, 470-472.

Fralick, P., 1999, Paleohydraulics of chute-and-pool structures in a Paleoproterozoic fluvial sandstone. *Sedim. Geol.*, **125**, 129-134.

Fukushima, Y., Parker, G. and Pantin, H.M., 1985, Prediction of ignitive turbidity currents in Scripps Submarine Canyon. *Mar. Geol.*, **67**, 55-81.

Gibbs, R.J., Matthews, M.D. and Link, D.A., 1971, The relationship between sphere size and settling velocity. *J. Sedim. Petrol.*, **41**, 7-18.

Gilbert, G.K., 1914, The transportation of debris by running water. *U. S. Geol. Surv. Prof. Paper*, **86**, 263pp.

Gilbert, I.M., Pudsey, C.J. and Murray, J.W., 1998, A sediment record of cyclic bottom-current variability from the northwest Weddel Sea. *Sedim. Geol.*, **115**, 185-214.

Gladstone, C., Phillips, J.C. and Sparks, R.S.J., 1998, Experiments on bidisperse, constant-

volume gravity currents: propagation and sediment deposition. *Sedimentology*, **45**, 833-843.

Hall, J.K., 1979, Sediment waves and other evidence of paleo-bottom currents at two locations in the deep Arctic Ocean. *Sedim. Geol.*, **23**, 269-299.

Hallworth, M.A., Phillips, C., Huppert, H.E. and Sparks, R.S.J., 1993, Entrainment in turbulent gravity currents. *Nature*, **362**, 829-831.

Hand, B.M., 1969, Antidunes as trochoidal waves. *J. Sedim. Petrol.*, **39**, 1302-1309.

Hand, B.M., 1974, Supercritical flow in density currents. *J. Sedim. Petrol.*, **44**, 637-648.

Hand, B.M., 1975, Supercritical flow in density currents: reply. *J. Sedim. Petrol.*, **45**, 750-753.

Hand, B.M., Wessell, J.M. and Hayes, M.O., 1969, Antidunes in the Mount Toby conglomerate (Triassic), Massachusetts. *J. Sedim. Petrol.*, **39**, 1310-1316.

Hand, B.M., Middleton, G.V. and Skipper, K., 1972, Antidune cross-stratification in a turbidite sequence, Cloridorme Formation, Gaspe, Quebec. *Sedimentology*, **18**, 135-138.

Hay, A.E., 1983, On the frontal speeds of internal gravity surges on sloping boundaries. *J. Geophys. Res.*, **88**, 751-754.

Hersey, J.B., 1965, Sediment ponding in the deep sea. *Geol. Soc. Am. Bull.*, **76**, 1251-1260.

Hess, G.R. and Normark, W.R., 1976, Holocene sedimentation history of the major fan valleys of Monterey Fan. *Mar. Geol.*, **22**, 233-251.

Hieke, W., 1984, A thick Holocene homogenite from the Ionian Abyssal Plain (eastern Mediterranean). *Mar. Geol.*, **55**, 63-78.

Hiscott, R.N., 1994, Loss of capacity, not competence, as the fundamental process governing deposition from turbidity currents. *J. Sedim. Res.*, **A64**, 209-214.

Howe, J.A., 1996, Turbidite and contourite sediment waves in the northern Rockall Trough, North Atlantic Ocean. *Sedimentology*, **43**, 219-234.

Howe, J.A., Livermore, R.A. and Maldonado, A., 1998, Mudwave activity and current-controlled sedimentation in Powell Basin, northern Weddell Sea, Antarctica. *Mar. Geol.*, **149**, 229-241.

Huppert, H.E., 1982, The propagation of two-dimensional and axisymmetric viscous gravity currents over a rigid horizontal surface. *J. Fluid Mech.*, **121**, 43-58.

Huppert, H.E. and Simpson, J.E., 1980, The slumping of gravity currents. *J. Fluid Mech.*, **99**, 785-799.

Huppert, H.E., Turner, J.S. and Hallworth, M.A., 1993, Sedimentation and mixing of a turbulent fluid suspension: a laboratory study. *Earth Planet. Sci. Lett.*, **114**, 259-267.

Jacobi, R.D. and Mrozowski, C.L., 1979, Sediment slides and sediment waves in the Bonin Trough, western Pacific. *Mar. Geol.*, **29**, M1-M9.

Jacobi, R.D., Rabinowitz, P.D. and Embley, R.W., 1975, Sediment waves on the Moroccan continental rise. *Mar. Geol.*, **19**, M61-M67.

Johnson, D.A, 1984, The Vema Channel: physiography, structure, and sediment-current interactions. *Mar. Geol.*, **58**, 1-34.

Johnson, D.A. and Damuth, J.E., 1979, Deep thermohaline flow and current-controlled sedimentation in the Amirante Passage: western Indian Ocean. *Mar. Geol.*, **33**, 1-44.

Johnson, D.A., Ledbetter, M.T., Tappa, E. and Thunell, R., 1984, Late Tertiary/Quarternary magnetostratigraphy and biostratigraphy of Vema Channel sediments. *Mar. Geol.*, **58**, 89-100.

Kennedy, J.F., 1963, The mechanics of dunes and antidunes in erodible-bed channels. *J. Fluid Mech.*, **16**, 521-544.

Kennedy, J.F., 1969, The formation of sediment ripples, dunes, and antidunes. *Ann. Rev. Fluid Mech.*, **1**, 147-168.

Kersey, D.G. and Hsü, K., 1976, Energy relations of density-current flows: an experimental investigation. *Sedimentology*, **23**, 761-789.

Kirwan, A.D., Doyle, L.J., Bowles, W.D. and Brooks, G.R., 1986, Time-dependent hydrodynamic models of turbidity currents analyzed with data from the Grand Banks and Orleansville evenets. *J. Sedim. Petrol.*, **56**, 379-386.

Klaus, A. and Ledbetter, M.T., 1988, Deep-sea sedimentary processes in the Argentine Basin revealed by high-resolution seismic records (3.5 kHz echograms). *Deep-Sea Res.*, **35**, 899-917.

Kneller, B.C., 1995, Beyond the turbidite paradigm: physical models for deposition of turbidites and their implications for reservoir prediction. In: *Characterization of deep marine clastic systems* (Ed. by D.J. Prosser and A. Hartley), *Spec. Publ. Geol. Soc. Lond.*, 31-49.

Kneller, B., Edwards, D., McCaffrey, W. and Moore, R., 1991, Oblique reflection of turbidity currents. *Geology*, **19**, 250-252.

Kolla, V., Moore, D.G. and Curray, J.R., 1976, Recent bottom-current activity in the deep western Bay of Bengal. *Mar. Geol.*, **21**, 255-270.

Kolla, V., Eittreim, S., Sullivan, L., Kostecki, J.A. and Burckle, L.H., 1980, Current- controlled, abyssal microtopography and sedimentation in Mozambique Basin, southwest Indian Ocean. *Mar. Geol.*, **34**, 171-206.

Kolla, V., Buffler, R.T. and Ladd, J.W., 1984, Seismic stratigraphy and sedimentation of Magdalena Fan, southern Colombian Basin, Caribbean Sea. *Am. Assoc. Petrol. Geol. Bull.*, **68**, 316-332.

Komar, P.D., 1969, The channelized flow of turbidity currents with application to Monterey deep-sea fan channel. *J. Geophys. Res.*, **74**, 4544-4558.

Komar, P.D., 1970, The competence of turbidity current flow. *Geol. Soc. Am. Bull.*, **81**, 1555-1562.

Komar, P.D., 1971, Hydraulic jumps in turbidity currents. *Geol. Soc. Am. Bull.*, **82**, 1477-1488.

Komar, P.D., 1972, Relative significance of head and body spill from a channelized turbidity current. *Geol. Soc. Am. Bull.*, **83**, 1151-1156.

Komar, P.D., 1973, Continuity of turbidity current flow and systematic variations in deep-sea channel morphology. *Geol. Soc. Am. Bull.*, **84**, 3329-3338.

Komar, P.D., 1975, Supercritical flow in density currents: a discussion. *J. Sedim. Petrol.*, **45**,

747-749.

Komar, P.D., 1985, The hydraulic interpretation of turbidites from their grain sizes and sedimentary structures. *Sedimentology*, **32**, 395-407.

Kostaschuk, R.A., Luternauer, J.L., McKenna, G.T. and Moslow, T.F., 1991, Sediment transport in a submarine channel system: Fraser River Delta, Canada. *J. Sedim. Petrol.*, **62**, 273-282.

Kuvaas, B. and Leitchenkov, G., 1992, Glaciomarine turbidite and current controlled deposits in Prydz Bay, Antarctica. *Mar. Geol.*, **108**, 365-381.

Laval, A., Cremer, M, Beghin, P. and Ravenne, C., 1988, Density surges: two-dimensional experiments. *Sedimentology*, **35**, 73-84.

Lebreiro, S.M., McCave, I.N. and Weaver, P.P.E., 1997, Late Quarternary turbidite emplacement on the Horseshoe abyssal plain (Iberian margin). *J. Sedim. Res.*, **67**, 856-870.

Lewis, K.B., 1971, Slumping on a continental slope inclined at 1°-4°. *Sedimentology*, **16**, 97-110.

Linden, P.F. and Simpson, J.E., 1986, Gravity-driven flows in a turbulent fluid. *J. Fluid Mech.*, **172**, 481-497.

Long, R.R., 1954, Some aspects of the flow of stratified fluids II. experiments with a two-fluid system. *Tellus*, **6**, 97-115.

Lonsdale, P., 1975, Sedimentation and tectonic modification of Samoan archipelagic apron. *Am. Assoc. Petrol. Geol. Bull.*, **59**, 780-798.

Lonsdale, P. and Smith, S.M., 1980, "Lower insular rise hills" shaped by a bottom boundary current in the mid-Pacific. *Mar. Geol.*, **34**, M19-M25.

Lüthi, S., 1981, Experiments on non-channelized turbidity currents and their deposits. *Mar. Geol.*, **40**, 59-68.

Manley, P.L. and Flood, R.D., 1993, Project MUDWAVE. *Deep-Sea Res. II*, **40**, 851-857.

Marani, M. Argnani, A., Roveri, M. and Trincardi, F., 1993, Sediment drifts and erosional

surfaces in the central Mediterranean: seismic evidence of bottom-current activity. *Sedim. Geol.*, **82**, 207-220.

Marjanac, T., 1990, Reflected sediment gravity flows and their deposits in flysch of Middle Dalmatia, Yugoslavia. *Sedimentology*, **37**, 921-929.

Markl, R.G., Bryan, G.M. and Ewing, J.I., 1970, Structure of the Blake-Bahama Outer Ridge. *J. Geophys. Res.*, **75**, 4539-4555.

McCave, I.N. and Swift, S.A., 1976, A physical model for the rate of deposition of fine-grained sediments in the deep sea. *Geol. Soc. Am. Bull.*, **87**, 541-546.

Middleton, G.V., 1965, Antidune cross-bedding in a large flume. *J. Sedim. Petrol.*, **35**, 922-927.

Middleton, G.V., 1966a, Experiments on density and turbidity currents I. motion of fluid. *Can. j. Earth Sci.*, **3**, 523-546.

Middleton, G.V., 1966b, Experiments on density and turbidity currents II. uniform flow of density currents. *Can. j. Earth Sci.*, **3**, 627-637.

Middleton, G.V., 1966c, Small-scale models of turbidity currents and the criterion for auto-suspension. *J. Sedim. Petrol.*, **36**, 202-208.

Middleton, G.V., 1967, Experiments on density and turbidity currents III. deposition of sediment. *Can. j. Earth Sci.*, **4**, 475-505.

Middleton, G.V., 1993, Sediment deposition from turbidity currents. *Ann. Rev. Earth Planet. Sci.*, **21**, 89-114.

Middleton, G.V. & Southard, J.B., 1984, *Mechanics of sediment movement*, 2nd edition. *SEPM short course*, **3**, 342pp.

Middleton, G.V. and Neal, W.J., 1989, Experiments on the thickness of beds deposited by turbidity currents. *J. Sedim. Petrol.*, **59**, 297-307.

Miles, J.W., 1968, Lee waves in a stratified flow. Part 2. Semi-circular obstacle. *J. Fluid Mech.*, **33**, 803-814.

Muck, M.T. and Underwood, M.B., 1990, Upslope flow of turbidity currents: A comparison

among field observations, theory, and laboratory models. *Geology*, **18**, 54-57.

Mulder, T., Syvitski, J.P.M. and Skene, K.I., 1998, Modeling of erosion and deposition by turbidity currents generated at river mouths. *J. Sedim. Res.*, **68**, 124-137.

Nakajima, T., 1996, Turbidite sedimentation along the Toyama Deep Sea Channel in the Japan Sea. Doctoral dissertation, Kyoto University, 108pp.

Nakajima, T., Satoh, M. and Okamura, Y., 1998, Channel-levee complexes, terminal deep-sea fan and sediment wave fields associated with the Toyama Deep-Sea Channel system in the Japan Sea. *Mar. Geol.*, **147**, 25-41.

Nardin, T.R., 1983, Late Quarternary depositional systems and sea level change---Santa Monica and San Pedro Basins, California continental borderland. *Am. Assoc. Petrol. Geol. Bull.*, **67**, 1104-1124.

Noh, Y. and Fernando, H.J.S., 1992, The motion of a buoyant cloud along an incline in the presence of boundary mixing. *J. Fluid Mech.*, **235**, 557-577.

Normark, W.R., Hess, G.R., Stow, D.A.V. and Bowen, A.J., 1980, Sediment waves on the Monterey Fan levee: a preliminary physical interpretation. *Mar. Geol.*, **37**, 1-18.

Pantin, H.M., 1979, Interaction between velocity and effective density in turbidity flow: phase-plane analysis, with criteria for autosuspension. *Mar. Geol.*, **31**, 59-99.

Pantin, H.M. and Leeder, M.R., 1987, Reverse flow in turbidity currents: the role of internal solitons. *Sedimentology*, **34**, 1143-1155.

Parker, G., 1982, Conditions for the ignition of catastrophically erosive turbidity currents. *Mar. Geol.*, **46**, 307-327.

Parker, G., Fukushima, Y. and Pantin, H.M., 1986, Self-accelerating turbidity currents. *J. Fluid Mech.*, **171**, 145-181.

Pickering, K.T. and Hiscott, R.N., 1985, Contained (reflected) turbidity currents from the Middle Ordovician Cloridorme Formation, Quebec, Canada: an alternative to the antidune hypothesis. *Sedimentology*, **32**, 373-394.

Piper, D.J.W. and Savoye, B., 1993, Processes of late Quarternary turbidity current flow and deposition on the Var deep-sea fan, north-west Mediterranean Sea. *Sedimentology*, **40**, 557-582.

Piper, D.J.W., Shor, A.N. and Hughes Clark, J.E., 1988, The 1929 "Grand Banks" earthquake, slump, and turbidity current. In: *Sedimentologic consequences of convulsive geologic events* (Ed. by Clifton, H.E.). *Geol. Soc. Am. Spec. Pap.*, **229**, 77-92.

Piper, D.J.W., Hiscott, R.N. and Normark, W.R., 1996, Outcrop-scale acoustic facies analysis and latest Quarternary development of Hueneme and Dume submarine fans, offshore California. *Sedimentology*, **46**, 47-78.

Prave, A.R. and Duke, W.L., 1990, Small-scale hummocky cross-stratification in turbidites: a form of antidune stratification?. *Sedimentology*, **37**, 531-539.

Queney, P., 1948, The problem of air flow over mountains: a summary of theoretical studies. *Bull. Am. Meteorol. Soc.*, **29**, 16-26.

Reynolds, A.J., 1965, Waves on the erodible bed of an open channel. *J. Fluid Mech.*, **22**, 113-133.

Reynolds, S., 1987, A recent turbidity current events, Hueneme Fan, California: reconstruction of flow properties. *Sedimentology*, **34**, 129-137.

Ricci Lucci, F. and Valmori, E., 1980, Basin-wide turbidites in a Miocene, over-supplied deep-sea plain: a geometrical analysis. *Sedimentology*, **27**, 241-270.

Richards, P.C., Ritchie, J.D. and Thomson, A.R., 1987, Evolution of deep-water climbing dunes in the Rockall Trough --- implications for overflow currents across the Wyville-Thomson Ridge in the (?)late Miocene. *Mar. Geol.*, **76**, 177-183.

Roberts, D.G. and Kidd, R.B., 1979, Abyssal sediment wave field on Feni Ridge, Rockall Trough: long-range sonar studies. *Mar. Geol.*, **33**, 175-191.

Rona, P.A., 1969, Linear "lower continental rise hills" off Cape Hatteras. *J. Sedim. Petrol.*, **39**, 1132-1141.

Rottman, J.W. and Simpson, J.E., 1983, Gravity currents produced by instantaneous releases of a heavy fluid in a rectangular channel. *J. Fluid Mech.*, **135**, 95-110.

Rust, B.R. and Gibling, M.R., 1990, Three-dimensional antidunes as HCS mimics in a fluvial sandstone: the Pennsylvanian South Bar Formation near Sydney, Nova Scotia. *J. Sedim. Petrol.*, **60**, 540-548.

Sanders, J.E., 1965, Primary sedimentary structures formed by turbidity currents and related resedimentation mechanisms. In: *Primary Sedimentary Structures and their Hydrodynamic Interpretation* (Ed. by G.V. Middleton), *SEPM spec. publ.*, **12**, 192-220.

Schmincke, H., Fisher, R.V. and Waters, A.C., 1973, Antidune and chute and pool structures in the base surge deposits of the Laacher See are, Germany. *Sedimentology*, **20**, 553-574.

Shanmugam, G., 1997, The Bouma Sequence and the turbidite mind set. *Earth-Sci. Rev.*, **42**, 201-229.

Siegenthaler, C., Hsü, K.J. and Kleboth, P., 1984, Longitudinal transport of turbidity currents---a model study of Horgen events. *Sedimentology*, **31**, 187-193.

Simpson, J.E., 1982, Gravity currents in the laboratory, atmosphere, and ocean. *Ann. Rev. Fluid Mech.*, **14**, 213-234.

Simpson, J.E., 1986, Mixing at the front of a gravity current. *Acta Mechanica*, **63**, 245-253.

Simpson, J.E., 1997, *Gravity currents in the environments and the laboratory*, 2nd edition. Cambridge University Press, Cambridge, 244pp.

Simpson, J.E. and Britter, R.E., 1979, The dynamics of the head of a gravity current advancing over a horizontal surface. *J. Fluid Mech.*, **94**, 477-495.

Skipper, K., 1971, Antidune cross-stratification in a turbidite sequence, Cloridorme Formation, Gaspe, Quebec. *Sedimentology*, **17**, 51-68.

Skipper, K. and Bhattacharjee, S.B., 1978, Backset bedding in turbidites: a further example from the Cloridorme Formation (Middle Ordovician), Gaspe, Quebec. *J. Sedim. Petrol.*, **48**, 193-202.

Stacey, M.W. and Bowen, A.J., 1988, The vertical structure of density and turbidity currents: theory and observations. *J. Geophys. Res.*, **93**, 3528-3542.

Stoker, M.S., Akhurst, M.C., Howe, J.A. and Stow, D.A.V., 1998, Sediment drifts and contourites on the continental margin off northwest Britain. *Sedim. Geol.*, **115**, 33-51.

Stow, D.A.V., 1979, Distinguishing between fine-grained turbidites and contourites on the Nova Scotian deep-water margin. *Sedimentology*, **26**, 371-387.

Stow, D.A.V. and Bowen, A.J., 1980, A physical model for the transport and sorting of fine-grained sediment by turbidity currents. *Sedimentology*, **27**, 31-46.

Tucholke, B.E., 1977, Sedimentation processes and acoustic stratigraphy in the Bellingshausen Basin. *Mar. Geol.*, **25**, 209-230.

Van Andel, T.H. and Komar, P.D., 1969, Ponded sediments of the Mid-Atlantic Ridge between 22° and 22° north latitude. *Geol. Soc. Am. Bull.*, **80**, 1163-1190.

Van Tassel, J., 1981, Silver abyssal plain carbonate turbidite: flow characteristics. *J. Geol.*, **89**, 317-333.

Walker, R.G., 1967, Upper flow regime bed forms in turbidites of the Hatch Formation, Devonian of New York State. *J. Sedim. Petrol.*, **37**, 1052-1058.

Weatherly, G.L., 1993, On deep-current and hydrographic observations from a mudwave region and elsewhere in the Argentine Basin. *Deep-Sea Res. II*, **40**, 939-961.

Yagishita, K., 1994, Antidunes and traction-carpet deposits in deep-water channel sandstones, Cretaceus, British Colombia, Canada. *J. Sedim. Res.*, **A64**, 34-41.

Yih, C., 1969, Stratified flows. *Ann. Rev. Fluid Mech.*, **1**, 73-110.

Yokokawa, M., Masuda, F., Sakai, T., Endo, N. and Kubo, Y., 1999, Sedimentary structures generated in upper-flow-regime with sediment supply: Antidune cross-stratification (HCS mimics) in a flume. *Proc. Int. symp. of Prof. K.O. Emery Commemorative Workshop on Land-Sea Link in Asia*, 409-414.

Zeng, J. and Lowe, D.R., 1997a, Numerical simulation of turbidity current flow and

sedimentation: I. Theory. *Sedimentology*, **44**, 67-84.

Zeng, J. and Lowe, D.R., 1997b, Numerical simulation of turbidity current flow and sedimentation: II. Results and geological applications. *Sedimentology*, **44**, 85-104.